Article:
Kahraman, I., Uysal, N., Subaşı, Ç et al. (2026) Assessing and quantifying variability across vacuum-assisted resin infusion variants for aerospace-grade composite manufacturing. Polymer Composites. ISSN: 0272-8397

https://doi.org/10.1002/pc.71180

Polymer Composites

WILEY | spe INSPIRING PLASTICS PROFESSIONALS

RESEARCH ARTICLE OPEN ACCESS

Assessing and Quantifying Variability Across Vacuum-Assisted Resin Infusion Variants for Aerospace-Grade Composite Manufacturing

Ilhan Kahraman[1] | Nilperi Uysal[2] | Çağlar Subaşı[3] | Selin Dursun[4] | Muhammet İskender[1] | Özgü Çalın[1] | Uğur Şimşir[5] | Hatice S. Sas[6] | A. Tuğrul Seyhan[1,7]

[1]Department of Materials Science and Engineering, Eskisehir Technical University (ESTU), Iki Eylul Campus, Eskisehir, Turkey | [2]Turkish Petroleum International Company Inc. (TPIC), Ankara, Türkiye | [3]Department of R & D, Eskim Chemical Industry and Trade Inc, Eskisehir, Turkey | [4]BUTEKOM Composite Research Center, Demirtaş Dumlupınar OSB, Bursa, Turkey | [5]USEL Makina, İmes Sanayi Sitesi, İstanbul, Türkiye | [6]School of Mechanical, Aerospace and Civil Engineering, The University of Sheffield, Sheffield, UK | [7]Composite Materials Manufacturing Science Laboratory (CMMSL), research Center for Advanced Technologies (ITAM), Eskisehir Technical University (ESTU), Eskisehir, Turkey

Correspondence: A. Tuğrul Seyhan (atseyhan@eskisehir.edu.tr)

Received: 7 February 2026 | **Revised:** 6 April 2026 | **Accepted:** 27 April 2026

Keywords: autoclave processing | fiber volume fraction | mechanical properties | resin transfer infusion (RTI) | VARTM

ABSTRACT

Conventional vacuum-assisted resin transfer molding (C-VARTM) is recognized as a cost-effective resin infusion technique for manufacturing large-scale composite structures. However, C-VARTM suffers from inherent limitations, notably non-uniform resin flow, uncontrolled vacuum levels that generate unstable pressure gradients, and variability in fiber compaction. These factors collectively reduce process repeatability and dimensional precision, posing a major constraint to qualifying C-VARTM laminates for aerospace applications. Therefore, identifying, understanding, and justifying the dominant sources of process variability is essential to enable reliable production of aerospace-grade composite structures at quality levels comparable to autoclave processing. In this study, C-VARTM, employing flow distribution media, vacuum bagging, and passive impregnation without auxiliary compaction, was used as the baseline. Several vacuum infusion variants, including pressure-driven vacuum infusion (PD-VARTM), vibration-assisted vacuum infusion (VAVI), controlled atmospheric pressure resin infusion (CAPRI), and the membrane-assisted vacuum infusion process (MAVIP), were evaluated in terms of laminate density, fiber volume fraction (FVF), void content, and thickness uniformity, quantified at the resin inlet and vacuum outlet. Flexural testing was conducted on all laminates to evaluate their structural performance against panels produced by the aerospace-qualified, Bombardier-patented resin transfer infusion (RTI) process, whose first successful laboratory scale implementation based on soft-stiff compaction concept is reported here, thereby addressing a key gap in the literature.

1 | Introduction

The use of stiff and damage-tolerant composite components is of critical importance in the aerospace industry. In this sector, carbon fiber–reinforced epoxy prepregs cured in autoclaves remain the dominant manufacturing route, as the combined application of elevated temperature and external pressure ensures effective laminate consolidation, low void content, and highly reproducible structural quality [1–9]. In addition, two critical aspects should be highlighted, particularly for primary load-bearing aerospace structures. First, prepreg systems typically enable straighter fiber alignment with minimal crimp compared to woven fabric reinforcements, leading to improved load transfer efficiency and higher strength properties. Second, the use of toughened resin systems in prepregs significantly enhances damage tolerance, especially under impact loading conditions. These factors contribute to

Highlights

- C-VARTM has FVF $\Delta = 6.7\%$ and flexural strength varied by 13% across the part.
- VAVI has FVF $\Delta = 10.3\%$ and peak flexural strength 803 MPa at the vacuum outlet.
- MAVIP has FVF $\Delta = 0.44\%$ and flexural strength 671–631 MPa as inlet and outlet
- PD-VARTM has FVF $\Delta = 1\%$ and flexural strength 714–747 MPa as inlet and outlet.
- RTI has FVF $> 55\%$ and $\Delta = 0.2\%$ flexural strength, 768 MPa and modulus > 54 GPa.

the superior mechanical performance and lightweight potential of prepreg-based composites and should be considered when benchmarking alternative manufacturing routes [4]. However, despite these advantages, autoclave processing is inherently constrained by part size and tooling limitations, while also requiring substantial capital investment, energy consumption, and operational costs [10–13]. These limitations have driven sustained research efforts toward alternative manufacturing strategies, most prominently out-of-autoclave (OoA) processing routes, which aim to achieve void contents below the critical 1%–2% threshold while offering reduced cost, simplified infrastructure, and improved scalability, thereby approaching autoclave-grade laminate quality [9–15]. These drawbacks have motivated sustained research efforts toward alternative manufacturing strategies, most prominently out-of-autoclave (OoA) processing routes that seek to achieve void contents below the critical 1%–2% threshold while offering reduced cost, simplified infrastructure, and improved scalability, with the aim of approaching autoclave-grade laminate quality [9–15]. Among the various OoA processes investigated over the past decades, vacuum-assisted resin transfer molding (VARTM) has surfaced one of the most promising candidates for manufacturing large-scale, high-performance composite structures for this purpose, whose utilization has already been proved and adopted in sectors such as military, civil infrastructure, wind energy, and marine applications [1–3]. In VARTM, vacuum pressure draws liquid resin into a dry fibrous preform while simultaneously evacuating entrapped air, thereby limiting surface porosity and internal void formation. However, VARTM is intrinsically prone to non-uniform consolidation [4, 5]. A thickness gradient frequently develops during infusion due to pressure loss along the flow path from the resin inlet to the vacuum outlet. This effect is primarily attributed to progressive relaxation of the vacuum bag as the resin front advances, particularly over long flow distances. Consequently, spatial variations in fiber volume fraction (FVF) arise, resulting in locally heterogeneous mechanical properties across the laminate [3–6]. Additionally, time-dependent changes in compaction pressure during infusion alter the local permeability of the fibrous preform, further amplifying thickness non-uniformity. Collectively, these characteristics lead to limited dimensional control, poor process repeatability, and inconsistent laminate consolidation [4, 5]. All these factors significantly hinder the qualification of VARTM for aerospace-grade applications, where strict tolerances and structural uniformity are mandatory. In contrast to autoclave-cured laminates, which benefit from uniform external pressure and precisely controlled thermal environments, VARTM-based composites are inherently more susceptible to void formation, resin-rich regions, and fiber misalignment. These defects compromise not only static mechanical performance but also long-term structural reliability and damage tolerance [1, 11, 14]. To lessen these shortcomings, a range of process modifications and auxiliary consolidation strategies has been proposed in the literature, targeting enhanced compaction uniformity, increased FVF, and reduced void content [14, 16–18]. Of all, one most widely discussed approach is resin bleeding, a post-impregnation flow-control technique in which excess resin is intentionally allowed to move forward after initial saturation, aiming at the promotion of prolonged evacuation period, benefiting from additional compaction under vacuum, potentially yielding denser and more uniform laminates. Nevertheless, resin bleeding often requires extra processing times that may exceed the initial mold-filling stage, introducing a critical trade-off between laminate quality and manufacturing efficiency, which is particularly problematic for large-scale or high-throughput production scenarios [14, 17]. The second other most considered approach as an alternative strategy involves connecting the resin reservoir to the vacuum line once full impregnation is achieved, aimed at effectively equalizing pressure between the inlet and outlet [18]. This configuration arrests further resin flow and stabilizes laminate thickness, leading to a more uniform FVF distribution. Despite its effectiveness for the sake of laminate geometry at the end of infusion, this approach inherently eliminates the pressure gradient immediately after resin breakthrough. As a result, the driving force for additional resin redistribution or further compaction vanishes, limiting the ability to correct for pre-existing thickness gradients. Further improvements in laminate quality have been attempted to be pursued through the application of external compaction pressure using active systems such as inflatable bladders, magnetically actuated clamps, or pressurized chambers [14–22]. These systems aim to supplement vacuum pressure during or after infusion, thereby enhancing fiber packing density and interlaminar contact. While conceptually attractive, their practical implementation is often restricted by component geometry, mold complexity, and scalability challenges, as achieving uniform pressure distribution over large or complex structures remains non-trivial. On the other hand, beyond thickness non-uniformity, void formation remains one of the most critical and persistent defect mechanisms in vacuum-infused composite laminates, particularly in mold systems lacking mechanical clamping [2, 3, 9, 10]. Even negligible increases in void content have been shown to cause disproportionate reductions in tensile, flexural, and interlaminar shear properties due to stress concentration effects and disruption of efficient fiber–matrix load transfer [6–9]. Voids may originate from incomplete air evacuation, resin mixing turbulence, vacuum leaks, or capillary resistance within densely packed fiber tows. In thick or geometrically complex laminates, stagnation of the resin front near the vacuum outlet further increases the likelihood of air entrapment and incomplete wet-out. If not adequately controlled, these micro-scale defects accumulate into severe structural weaknesses, rendering conventionally infused laminates unsuitable for safety-critical or high-performance applications. Given together, these limitations reveal a persistent gap between quality and performance in traditional vacuum-based composite manufacturing routes [14, 18, 19]. Addressing this gap has driven a shift toward next-generation infusion technologies that move beyond passive vacuum compaction. Emerging approaches increasingly rely on pressure modulation, active flow control, and integrated compaction strategies to achieve more

uniform impregnation, enhanced volatile removal, and consistent fiber consolidation [20–23]. By justifying voids, resin-rich zones, and interfacial defects while avoiding the high costs associated with autoclave processing and shelf life limited prepregs, these advanced methods preserve the scalability and flexibility of VARTM-type processes aimed at approaching prepreg-based, autoclave-level mechanical performance [24–27].

Within this context, the present study provides a systematic and comprehensive evaluation of advanced resin infusion techniques, namely CAPRI, MAVIP, PD-VARTM, and VAVI, benchmarking them against conventional C-VARTM, which involves using flow distribution media, vacuum bagging, and passive impregnation without auxiliary compaction. The principal objective herein is to assess their potential to approach the structural quality and consistency traditionally achieved through resin transfer infusion (RTI), a process patented by Bombardier and widely regarded as a reference standard for its prepreg-based, autoclave-processed attainable performance. To this end, six distinct infusion variants were experimentally implemented under controlled laboratory conditions, and key quality metrics, including laminate thickness uniformity, FVF, and void content, were rigorously quantified as indicators of consolidation efficiency and structural homogeneity. Complementary flexural testing was conducted to evaluate the influence of each processing variant on stiffness and load-bearing capability, properties of central relevance for structural composite applications. While previous studies have examined individual infusion techniques such as C-VARTM, CAPRI, or MAVIP in isolation or limited comparative frameworks, the present work represents, to the best of the authors' knowledge, the first direct, side-by-side comparison of emerging strategies such as PD-VARTM and VAVI within a unified experimental platform and against an RTI reference. This integrated methodology enables robust performance comparison across multiple infusion variants under identical material systems and testing protocols. Furthermore, the study makes a distinct methodological contribution by reporting the first documented fabrication of flat composite panels using RTI, thereby addressing a notable gap in the existing literature.

2 | Materials and Methods

2.1 | Materials

An aerospace-grade epoxy resin system consisting of EPIKOTE MGS LR285 and EPIKURE MGS LH287 (Momentive, Germany) was used as the matrix phase in all laminates. It exhibits a viscosity of approximately 700 mPa·s at the infusion temperature (20°C), with a pot life of about 80 min, providing a sufficiently wide processing window for complete impregnation. The components were mixed at the manufacturer-specified weight ratio of 100:30 (resin: hardener, w/w) using a mechanical stirrer at 300 rpm for 15 min to ensure homogeneity. The mixture was then degassed under vacuum for 15 min to remove entrapped air prior to infusion. Note that this resin system was selected due to its low viscosity and stable processing behavior, enabling consistent impregnation and minimizing variability across the different infusion routes, thus allowing a clearer assessment of process-induced effects such as FVF, void content, and thickness uniformity. In other words, despite not being representative of high-Tg aerospace-grade resins, it provides a controlled baseline for comparative process evaluation. The reinforcement was a 2×2 twill woven T300 carbon fiber fabric (200 g/m^2) supplied by TELATEKS Corp. (Türkiye). This fabric was selected for its balance of drapability and in-plane mechanical performance, making it well-suited to resin infusion. Composite panels were manufactured using four fabric plies stacked in a symmetric lay-up, yielding flat laminates and minimizing residual stresses.

2.2 | Production of Composite Laminates Supplemented by an Experimental Overview

2.2.1 | Conventional Vacuum-Assisted Resin Transfer Molding (C-VARTM)

C-VARTM is among the most widely adopted liquid composite molding routes, largely due to its low tooling cost, operational simplicity, and suitability for manufacturing large and/or geometrically complex structures. In a typical implementation, dry fiber preforms are placed on a single-sided tool and subsequently covered with a peel ply, a flow distribution medium, commonly applied over the full lay-up area, and a vacuum bag. After sealing, vacuum is applied to evacuate the cavity and to drive resin infiltration from a feed reservoir [2, 5, 12]. Figure 1 presents a schematic of the C-VARTM set-up together with an in-process photograph acquired during laminate manufacture in the present study. Resin transport is governed solely by vacuum pressure, while the distribution medium promotes rapid in-plane flow and facilitates uniform wet-out across the lay-up. Despite its practicality and established industrial relevance, C-VARTM is highly sensitive to flow non-uniformities, inlet/outlet positioning, and vacuum integrity. Following the transition of resin from the reservoir (initially at atmospheric pressure) into the porous preform, the advancing resin exerts hydrostatic pressure on the vacuum bag, thereby locally reducing the effective compaction pressure. Consequently, the pressure differential within the already impregnated region is partially neutralized, promoting relaxation of the previously consolidated fibrous bed through elastic, plastic, and hysteretic contributions. As the flow front progresses, resin pressure decreases along the flow path and the pressure differential gradually recovers toward the vent end, approaching the initial vacuum-driven gradient. In this work, after completion of infusion, a controlled bleeding step was applied for 15 min. The term, controlled bleeding step refers to a regulated resin outflow at the outlet to prevent excessive resin accumulation and to maintain a stable flow front during infusion. It does not imply intentional additional resin inflow to address dual-scale impregnation. Instead, the approach balances inlet supply and outlet evacuation, thereby promoting uniform in-plane flow while allowing sufficient time for through-thickness impregnation at the tow scale. This is particularly relevant for carbon fiber preforms, where dual-scale flow effects may lead to preferential macro-flow and delayed micro-impregnation within fiber tows. In the present study, this strategy was applied specifically in the C-VARTM process, where flow instabilities are more pronounced, to promote uniform impregnation while minimizing resin-rich regions and flow-induced defects. The laminates were then cured under vacuum at −0.9 kPa by heating from ambient

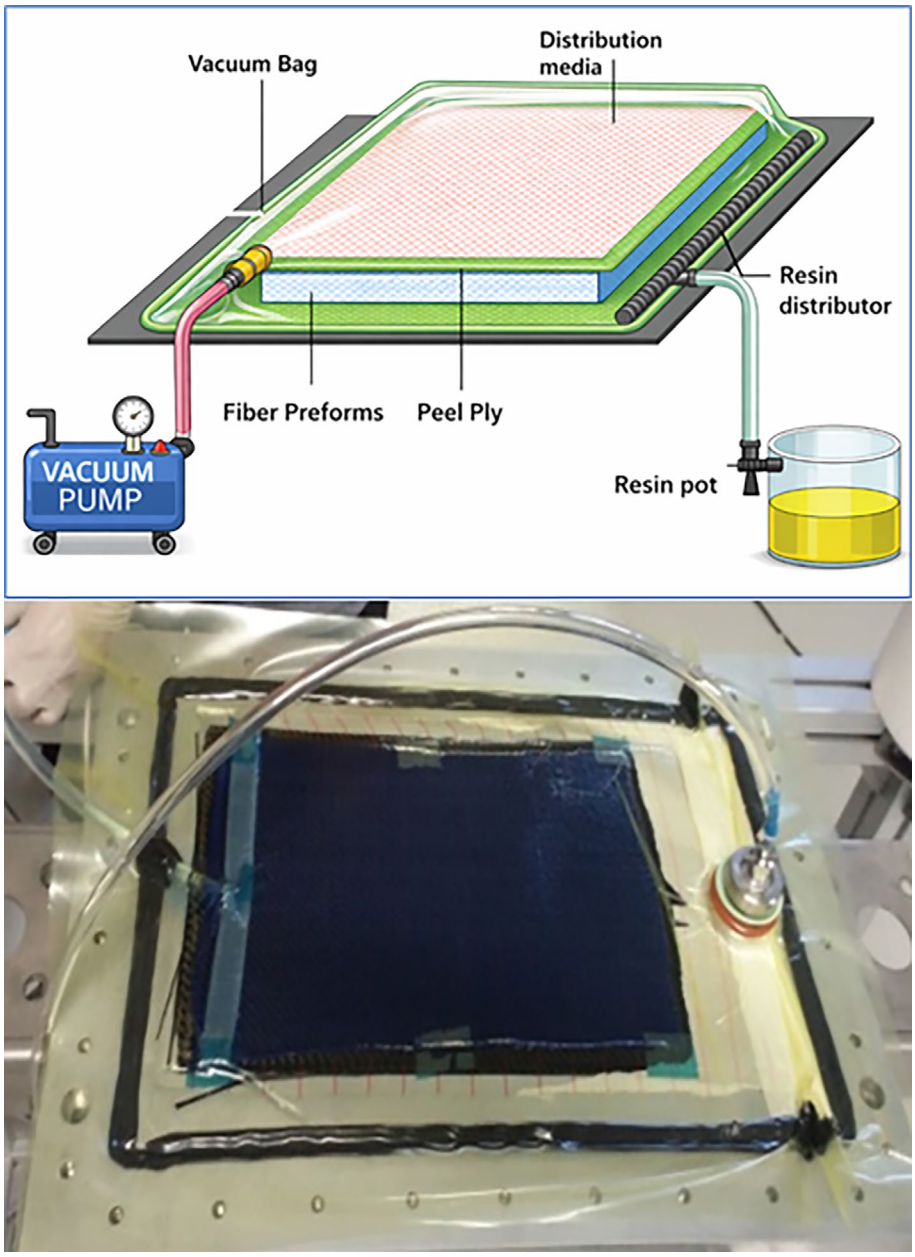

FIGURE 1 | Conventional schematic VARTM set-up and a photo taken during the production of the laminate.

to 60°C at 2°C min^{-1}, followed by a post-cure at 60°C for 15 h. All curing stages were conducted in a programmable convection oven and monitored using embedded thermocouples to verify spatially uniform temperature distribution.

2.2.2 | The Membrane-Assisted Vacuum Infusion Process (MAVIP)

MAVIP is an advanced VARTM variant developed by Airbus to address key shortcomings of conventional infusion, known as VAP, in the literature in some sources as well. Its defining feature is a semi-permeable membrane placed between the dry preform and the vacuum bag [25–27] This membrane permits evacuation of air and volatiles while blocking resin transport, thereby limiting resin bleed, improving degassing, and promoting more uniform consolidation. Vacuum is applied via a port located between the membrane and the vacuum bag, enabling homogeneous suction over the entire lay-up using a single outlet and eliminating the need for complex vacuum channel layouts. Figure 2 presents the MAVIP configuration together with an in-process photograph recorded during infusion. In the present study, a TPU-based VAP membrane supplied by Trans GmbH (Germany) was employed. MAVIP has been implemented in aerospace structures, including Airbus A400M cargo doors, A380 fuselage elements, and Eurofighter wing flap tracks, highlighting its industrial maturity and structural robustness [25]. Literature reports further indicate that E-glass/epoxy laminates manufactured by MAVIP can achieve void contents comparable to autoclave-cured counterparts, together with a 77% reduction in thickness gradient [27]. In addition, low-frequency mechanical vibration has been proposed as a process aid, with reported effects on filling time, flow velocity, and void formation. Operationally, MAVIP requires careful control because

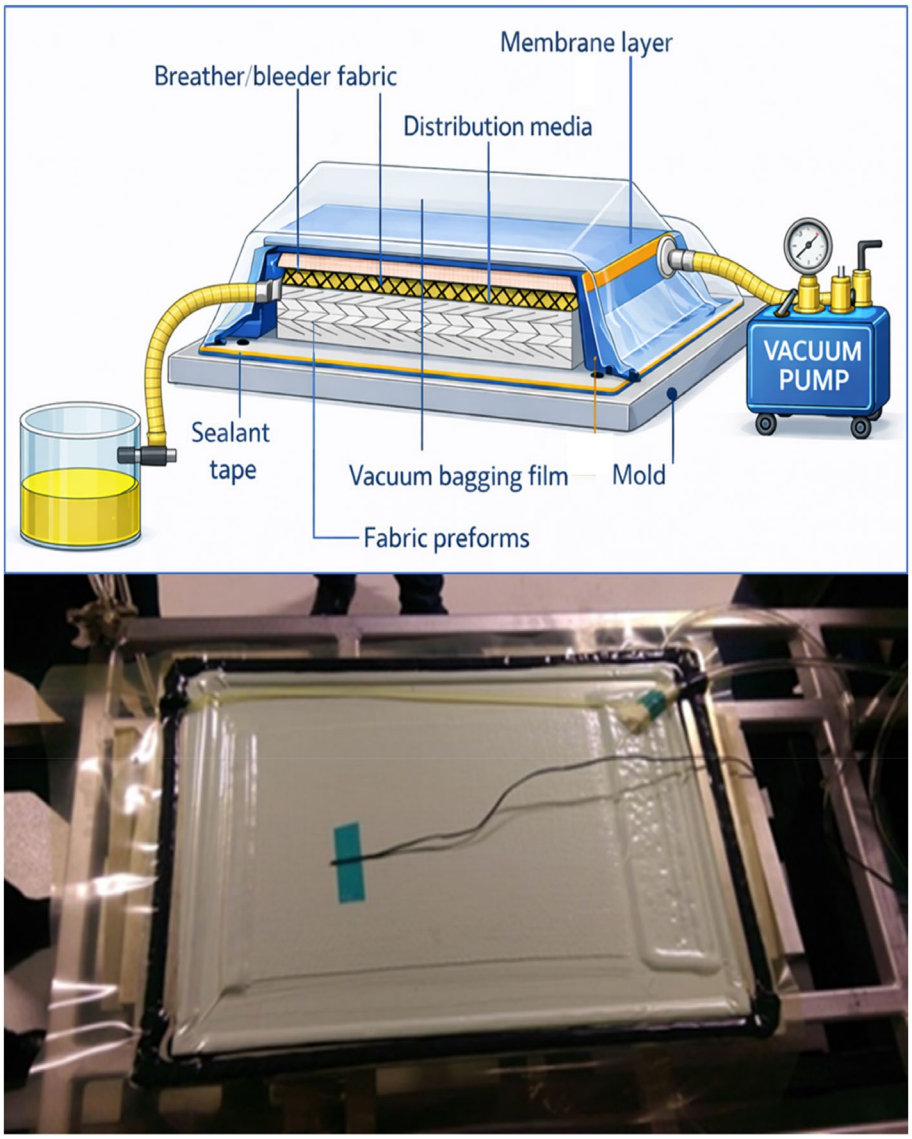

FIGURE 2 | MAVIP process schematic set up and a photo taken during the production of the laminate.

the vacuum field beneath the membrane remains stable and may sustain resin flow even after full saturation unless the inlet is closed. If infusion continues unchecked, resin-rich regions can develop, leading to increased laminate thickness and reduced FVF. To avoid this, temperature and resin-arrival sensors were used in combination in the present work. After flow termination, the same curing procedure as in C-VARTM was applied.

2.2.3 | Controlled Atmospheric Pressure Resin Infusion (CAPRI)

CAPRI is an advanced VARTM-derived process developed by Boeing to enhance fiber-bed consolidation and reduce laminate thickness variability. In contrast to conventional C-VARTM, CAPRI incorporates a pre-infusion debulking stage based on repeated compaction–relaxation cycles. Full vacuum is first applied to compact the dry preform and is then partially released to allow controlled elastic recovery of the bag. This sequence improves nesting and fiber alignment and reduces preform spring-back, thereby helping to minimize thickness differences between regions experiencing different local compaction states. A second distinguishing feature of CAPRI is the use of two vacuum levels. Full vacuum is applied at the vacuum outlet, while a partial vacuum is imposed at the resin inlet. This arrangement establishes a controlled pressure field in which the vacuum bag remains partially supported by atmospheric pressure during infusion, while resin is delivered under reduced pressure [20, 21]. As a result, debulking decreases interstitial void volume and facilitates subsequent impregnation, whereas controlled resin pressure impedes race-tracking, flow instabilities, and resin-rich regions, promoting a smoother flow front and more predictable saturation. Figure 3 illustrates the CAPRI set-up together with an in-process photograph acquired during manufacture in a programmable composite oven. Overall, compared with C-VARTM, CAPRI pressure management increases consolidation within the resin-impregnated region, which typically translates into higher FVF and a reduced thickness gradient. In the present study, debulking was performed using 80 compaction–relaxation cycles, with pressure ramped to 70 kPa within 30 s and subsequently reduced to approximately 10 kPa

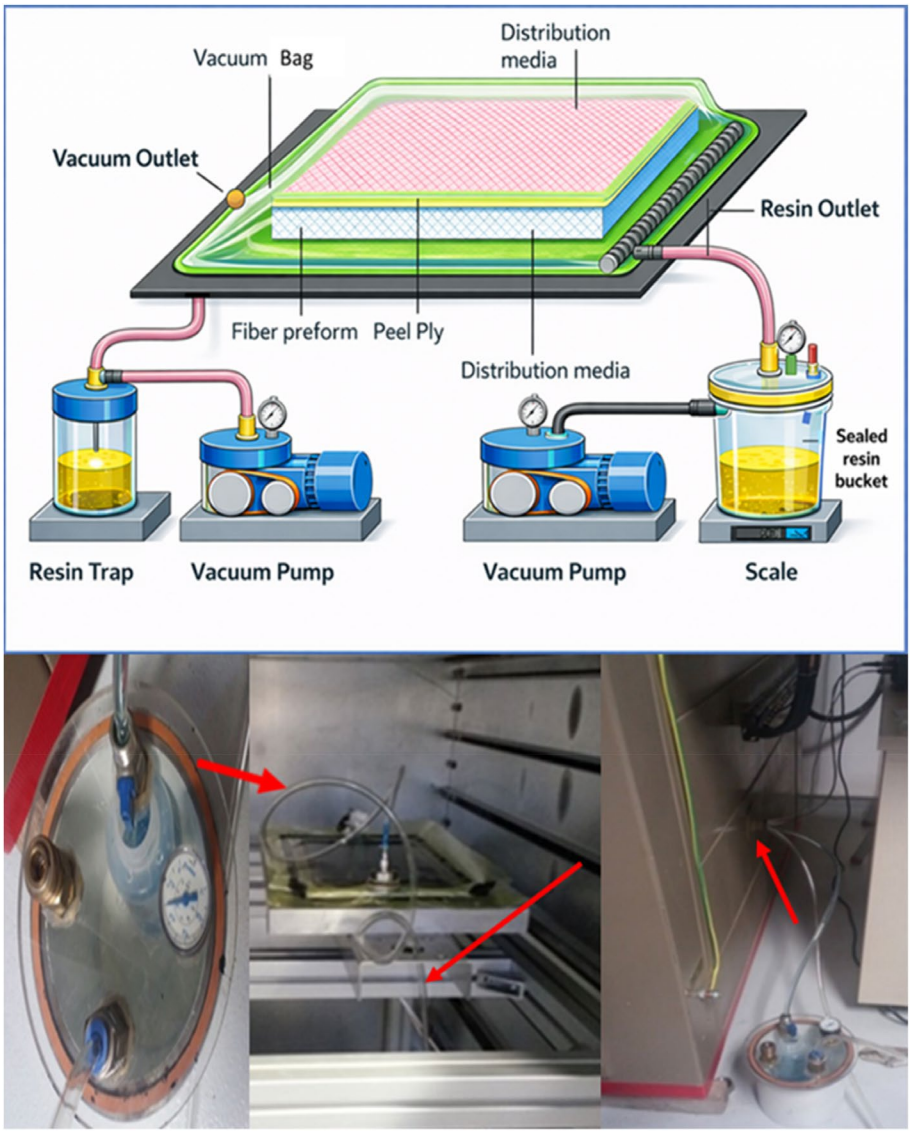

FIGURE 3 | CAPRI schematic setup, along with a photo taken underneath during the production of the sample part in a conventional composite oven. Red arrows show the pipeline for resin from outside to inside through the oven wall.

over 10 s to enhance ply relaxation and inter-ply conformity with a total infusion time of 28 min. The number of cycles was determined based on preliminary trials to achieve a stable and well-consolidated preform state, allowing sufficient preform stress relaxation between compaction stages while avoiding excessive fiber nesting. It is recognized that repeated debulking may reduce preform thickness and permeability due to nesting effects. However, within the selected cycle range, a balanced condition was achieved in which improved consolidation did not lead to a detrimental increase in infusion time. Moreover, to reduce through-thickness compaction gradients during infusion, a half-vacuum strategy was employed such that a partial vacuum of 35 kPa was applied to the infusion bucket while the outlet vacuum was maintained at 70 kPa, with the preform remaining partially compacted throughout resin delivery. Note that resin infusion was initiated immediately after the final debulking cycle to minimize preform relaxation and preserve the achieved compaction state. The laminates were then cured following the same procedure applied to the C-VARTM- and MAVIP-produced laminates.

2.2.4 | The Vibration-Assisted Vacuum Infusion (VAVI) Method

VAVI is an emerging liquid composite molding approach aimed at mitigating void formation in vacuum infusion. It applies low-frequency vibration, typically in the 30–100 Hz range, most effectively after infusion once the cavity is filled but prior to gelation. In the present study, VAVI was implemented as a vibration-assisted variant of C-VARTM. All processing parameters, including vacuum level, lay-up configuration, and infusion strategy, were kept identical to those of C-VARTM, with vibration being the only additional parameter introduced during the infusion stage. Literature reports indicate that 50 Hz vibration can reduce void content by more than 50% and decrease void count by 59%, accompanied by a slight increase in mean void size and a modest density increase attributed to improved fiber packing [26]. Mechanistically, vibration increases resin mobility, promotes degassing, and enhances fiber–resin contact in regions susceptible to air entrapment. The imposed oscillation introduces local pressure and shear fluctuations,

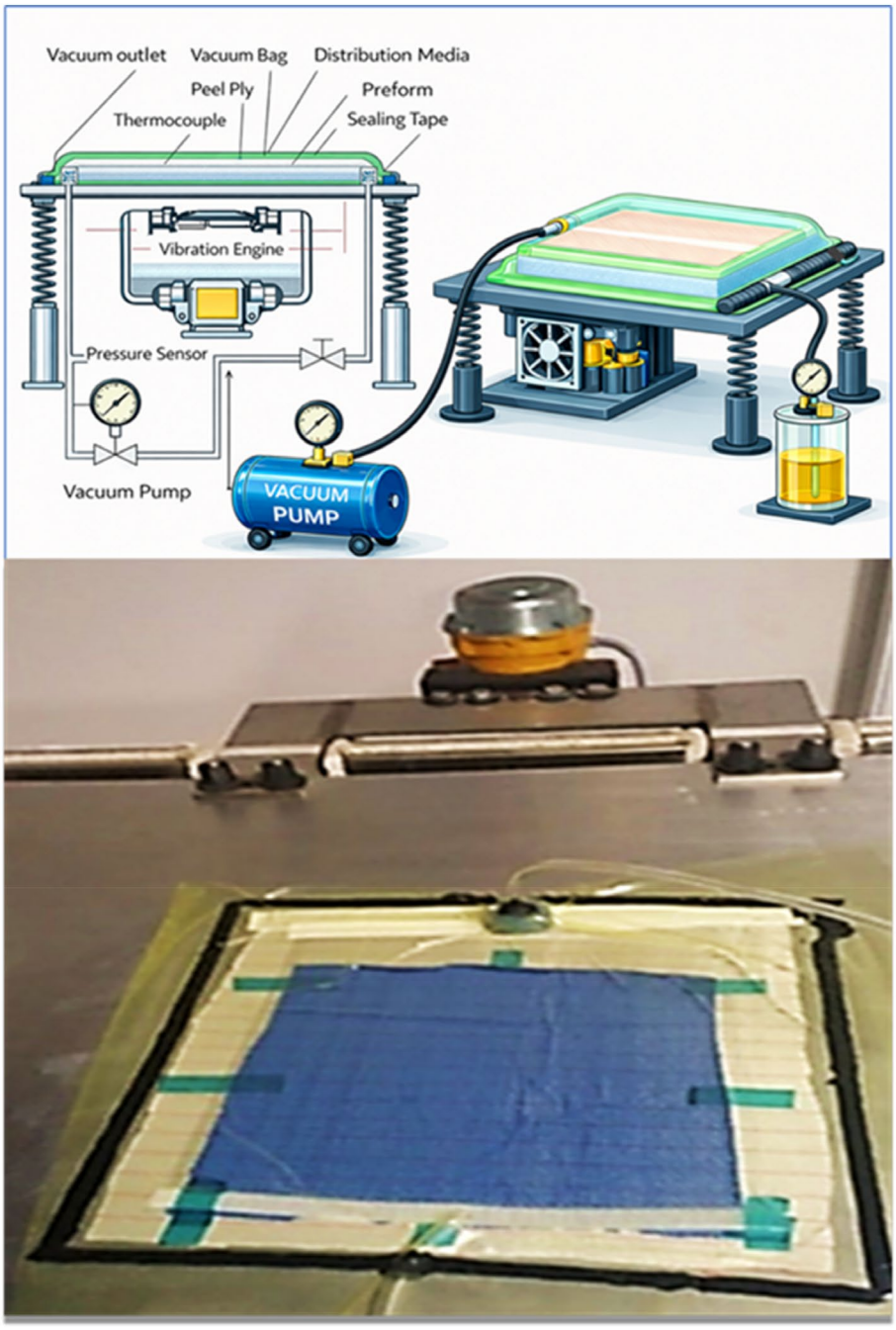

FIGURE 4 | VAVI schematic process set up and a photo taken during the production of the sample laminate.

which can reduce effective viscosity via mechanical thinning and mobilize microbubbles toward vacuum escape pathways. VAVI performance depends strongly on vibration frequency, amplitude, and timing relative to gelation. Early application may disturb the flow front and promote air injection or preferential flow channels, whereas late application can be ineffective due to elevated resin viscosity. Excessive excitation can also induce fiber washout, resin pooling, or local inter-ply separation. In the present study, a vibration motor was mounted near the steel tool, with its rotational axis aligned parallel to the flow-front direction. Figure 4 illustrates the experimental set-up together with an in-process photograph. The assembly was supported on four coil springs to minimize damping and ensure a stable oscillatory response, while the vibration frequency was controlled via the power supply. A frequency of 60 Hz was applied starting 25 min after flow onset and maintained until the end of the infusion stage. This parameter was selected based on prior experimental results reported in our previous study [25], which indicated improved resin infiltration and void reduction under this condition. The laminate was subsequently cured following the same procedure as the other variants.

2.2.5 | The Pressure-Driven VARTM (PD-VARTM)

PD-VARTM is a refined VARTM variant developed to address two recurring shortcomings of C-VARTM, namely non-uniform

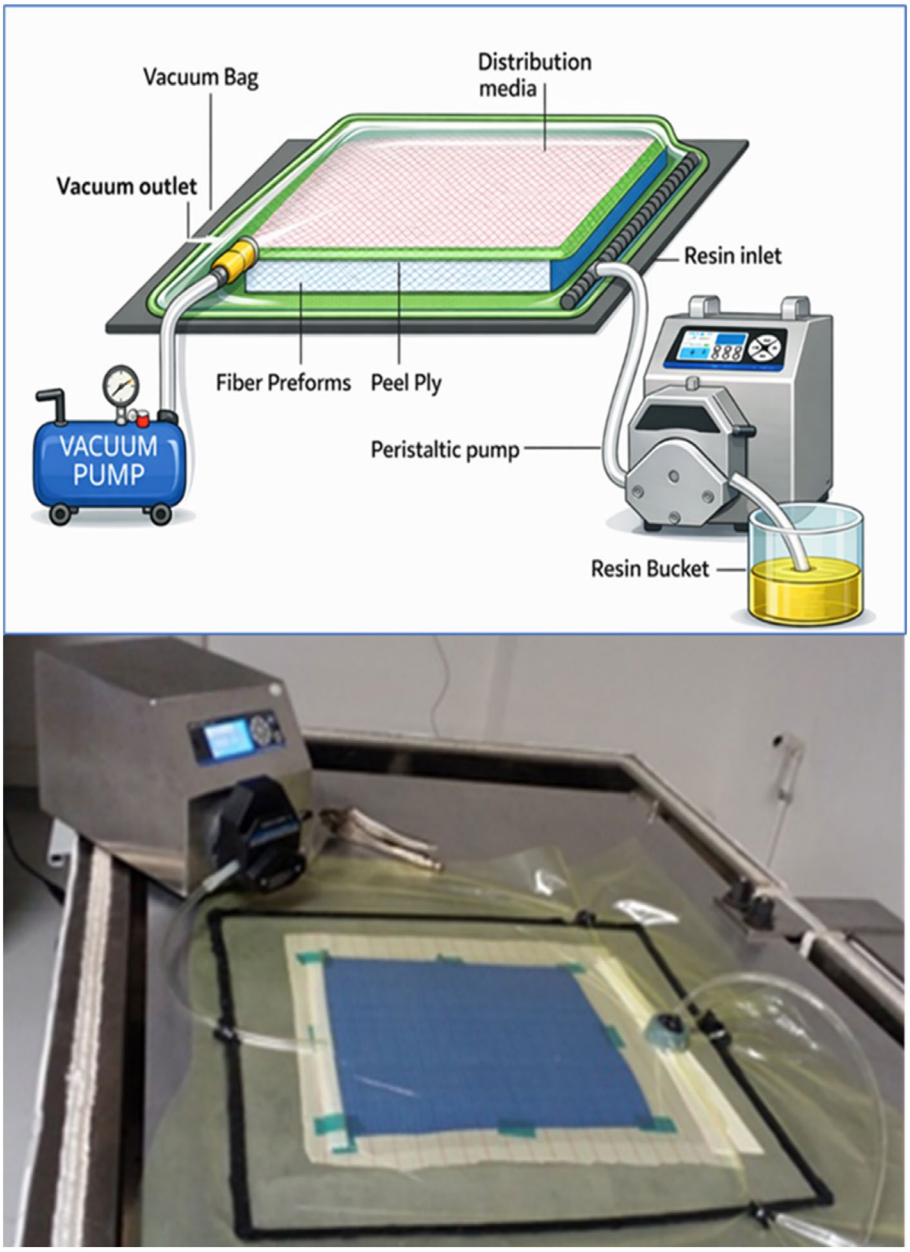

FIGURE 5 | PD-VARTM schematic illustration and a below photo taken during the process.

laminate thickness and limited process repeatability. In C-VARTM, resin transport relies solely on vacuum pressure, which can lead to fluctuating flow rates and unstable pressure gradients, particularly near the inlet, thereby promoting resin-rich regions, increasing local thickness, and increasing susceptibility to void entrapment [27]. PD-VARTM mitigates these effects by integrating a peristaltic pump to regulate resin delivery, reducing operator dependence, and improving process stability and reproducibility. Peristaltic pumps generate flow by sequentially compressing flexible tubing, enabling controlled, yet inherently pulsatile resin delivery. In this approach, the pump meters a prescribed volume of liquid resin into the mold within a defined dwell time window, assisting in promoting both in-plane impregnation and through-thickness wet-out of the fabric preform. The delivered resin quantity is primarily governed by pump speed, which is selected based on the specific fabric–resin system and the targeted panel thickness [28]. This configuration provides a stable, programmable flow rate and can accommodate even higher viscosity resins that are challenging to infuse using vacuum pressure alone. Figure 5 illustrates the PD-VARTM set-up together with an in-process photograph acquired during manufacture. In the present study, a variable-speed Masterflex L/S Easy-Load II peristaltic pump was installed in the feed line to implement a peristaltic-driven infusion configuration and to enable real-time control of inlet flow rate and pressure. The pump provides flow rates from 0.06 to 2300 mL min^{-1} over 1–600 rpm and was operated in cyclic mode using a programmable timer. A series of systematic preliminary trials were conducted by varying pump speed and on/off cycle durations to identify a stable operating window. These trials were qualitatively evaluated in terms of flow-front stability, absence of excessive resin accumulation near the inlet, and completion of mold filling without disturbing the preform architecture. After preliminary trials with different operating conditions, a setting of 500 rpm with on/off cycles of

15 s and 60 s, respectively, was selected as a suitable operating condition. This approach enabled controlled inlet delivery and stabilized mold pressure while maintaining the resin in a low-viscosity state during filling. The intermittent application of pressure was not maintained throughout the entire process but was reduced toward the final stages of filling, allowing partial vacuum bag relaxation under the prevailing vacuum conditions. Considering the restraining effect of the vacuum bagging system, this behavior prevented significant bag inflation. Accordingly, no decisive thickness variation was observed within the resolution of the measurements. The laminates were cured using the same procedure as for the other variants.

2.2.6 | Resin Transfer Infusion (RTI)

RTI is a patented, aerospace-qualified composite manufacturing route developed by Bombardier Aerospace for primary aircraft structures, including the C Series (now the Airbus A220) wing box. It provides a practical alternative to conventional resin transfer molding (RTM). While RTM is well known for producing medium-sized parts with high dimensional fidelity, its application to large aerospace structures is often constrained by the requirement for heavy matched tooling and high clamping capacity [29, 30]. RTI addresses this limitation by performing resin infusion under full vacuum in an unpressurised autoclave, followed by pressure-assisted consolidation within the same vessel. In the present study, the RTI route should be regarded as a laboratory-scale implementation inspired by the stiff–soft compaction concept reported in the literature, rather than as an exact duplication of Bombardier's proprietary industrial process. In RTI, the vacuum blanket refers to the multilayer, compliant bag-side assembly, including breather, distribution media, and locally stiff inserts, which governs vacuum distribution, resin-flow guidance, and pressure-assisted consolidation during autoclave processing [14, 16, 17, 28–32]. Figure 6 shows the RTI schematic together with a photo below showing the experimental configuration completed prior to the process with the cure cycle applied included. Unlike prepreg/autoclave processing, where refrigerated storage and strict out-life constraints can limit practical laminate thickness, RTI accommodates substantially thicker dry fiber stacks in a single cycle, reducing lay-up time, material waste, and handling complexity. Reported FVFs exceed 55% for laminates up to 1.25 in. thick, together with weight savings of 10% relative to metallic counterparts [29–31]. Thin aluminium was used to locally modify stiffness distribution and control resin flow behavior within the laminate.

In this study, the stiff–soft concept intrinsic to RTI was implemented using thin aluminium inserts (approximately 0.8–1.0 mm in thickness and 30 × 30 mm in planar dimensions) as locally stiff regions and conventional breather/bleeder materials with distribution media as compliant soft zones within the vacuum bag. This architecture was deliberately designed not only to enhance consolidation during the pressure stage but also to actively control local permeability and cavity compliance during the vacuum-assisted infusion phase. During vacuum-only infusion, the lay-up comprising fiber preforms, peel ply, and distribution media was enclosed within a tailored bagging assembly incorporating aluminium edge strips, central stiff patches, and corner inserts. The stiff elements were embedded within compliant, breather-based regions which, under vacuum, underwent slight deformation to form preferential high-permeability corridors. This facilitated stable flow-front progression, guided in-plane resin transport, and suppressed premature channel closure. Simultaneously, the corner inserts preserved local cavity height, ensuring a stable flow geometry until complete impregnation. As a result, the imposed permeability contrast and spatial variation in compliance enabled uniform in-plane flow while promoting through-thickness impregnation at the tow scale prior to gelation. Following complete impregnation under full vacuum, autoclave pressure was applied in a controlled manner once macroscopic flow had ceased and the resin had entered a pre-gel state, typically within the viscoelastic transition window near the G'–G'' crossover. At this stage, the resin retains sufficient mobility to respond to pressure, while bulk flow is effectively suppressed, thereby preventing fiber washout and preform distortion. Accordingly, the pressure stage does not contribute to primary filling, but instead governs consolidation and resin redistribution. The delayed pressure application ensures that consolidation occurs within the viscoelastic transition window, thus avoiding pressure-driven flow while enabling effective resin redistribution. Under autoclave loading, the stiffness contrast between stiff and compliant regions generates localized pressure gradients that drive controlled resin redistribution. The compliant zones compress more significantly, reducing resin-rich regions and directing excess resin toward adjacent low-pressure regions and compliant bleed pathways within the vacuum blanket architecture. At this stage, the resin exhibits a pressure-responsive viscoelastic behavior, enabling viscosity-governed squeeze flow and controlled redistribution. Meanwhile, the aluminium inserts undergo negligible deformation, reinforcing local pressure gradients and promoting fiber bed compaction. This coupled mechanism results in increased local FVF, improved thickness uniformity, and reduced structural heterogeneity across the laminate. RTI laminates were subsequently cured in an autoclave by heating from 20°C to 60°C at a rate of 2°C min^{-1}, consistent with the other process variants. During heating, the autoclave pressure was increased stepwise from 100 to 600 kPa at a rate of 50 kPa min^{-1}, with intermediate dwell periods of 5 min at 200 kPa and 10 min at 400 kPa to ensure pressure equilibration and controlled consolidation. A constant vacuum level of −90 kPa was maintained throughout both the infusion stage and the autoclave pressure cycle to preserve laminate compaction and facilitate the removal of entrapped air and volatiles. An isothermal dwell was then applied at 60°C and 600 kPa for 50 min under continuous vacuum, followed by controlled depressurization at 15 kPa min^{-1} and simultaneous cooling to ambient temperature. Finally, all laminates were post-cured at 60°C for 13 h in a convection oven to ensure consistent post-curing conditions and to equalize the thermal history across all process variants.

2.3 | Measurements of Composite Density, Fiber Volume Fraction, and Void Content

The density of each composite specimen was determined in accordance with ASTM D792-13 using the water-buoyancy method based on Archimedes' principle. Density measurements

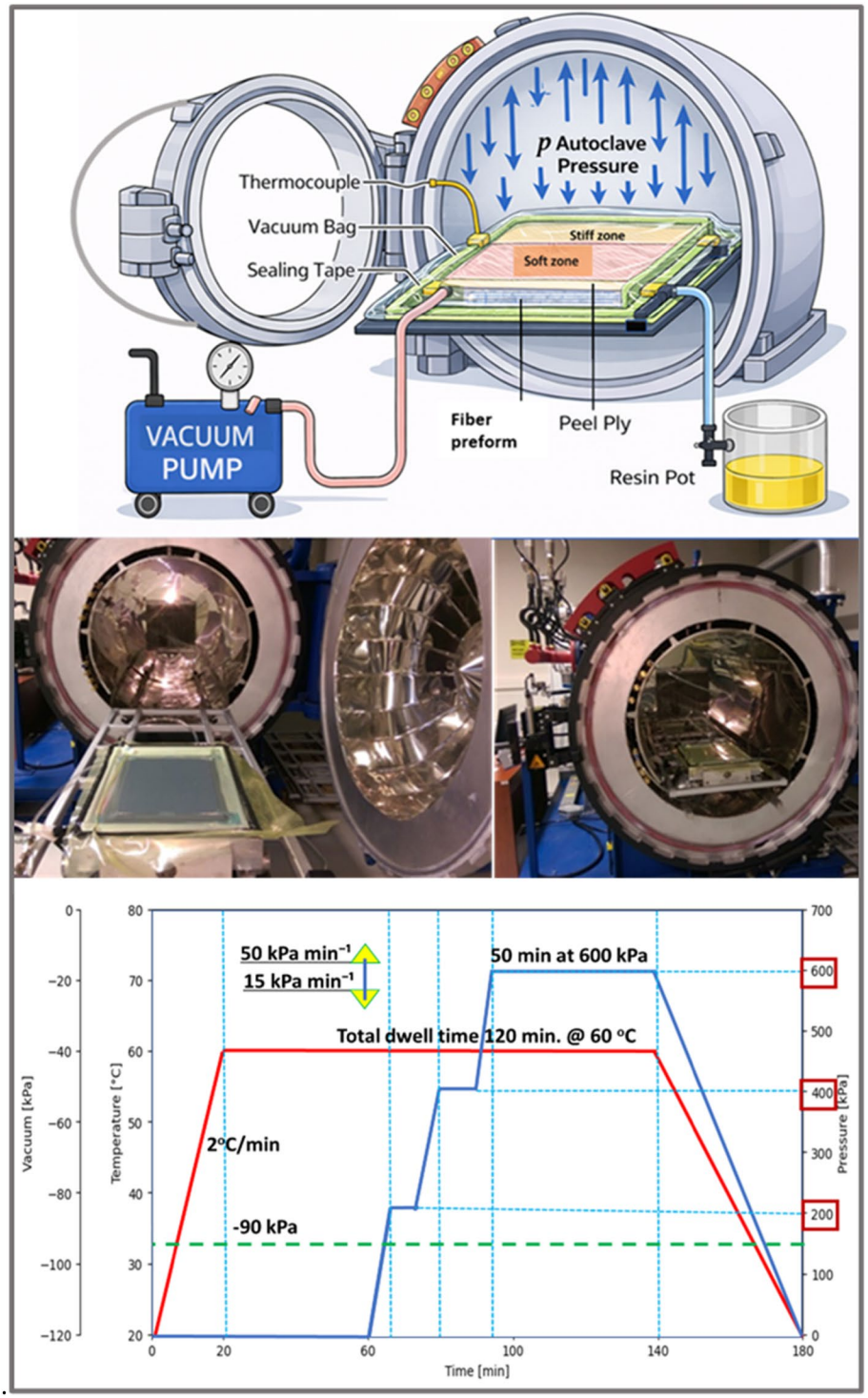

FIGURE 6 | Schematic representation of the RTI processing cycle, showing temperature, pressure, and vacuum profiles. Autoclave pressure is applied in a delayed, stepwise manner following complete impregnation.

were performed prior to mechanical testing to ensure consistency. Subsequently, three-point bending tests, ASTM D-790, were conducted to determine the flexural strength and flexural modulus of the composites. Fiber content was quantified using a thermogravimetric analysis (TGA)-based methodology. Composite specimens previously tested in flexure were sectioned into small cylindrical samples suitable for TGA pans. To systematically assess potential variations in resin distribution across the part, independent of the testing method, a minimum of five specimens were extracted from selected locations near the resin inlet and the vacuum outlet. This sampling protocol was designed to ensure statistical robustness and to capture spatial variability within the laminate. Consequently, it enables a representative evaluation of fiber to resin distribution and its direct influence on the resulting mechanical and thermal performance. Moreover, it should be noted that only a single panel was manufactured for each process in the present study, and that a comprehensive statistical assessment among multiple

panels was beyond the scope of this work, putting aside part-to-part variability that may have influenced the observed results to some extent, but not decisively. Nevertheless, the adopted sampling approach, involving specimens taken from distinct regions of each panel, provides a reasonable basis for capturing in-panel variability. All samples were cut by waterjet machining to maintain dimensional accuracy and minimize thermal or mechanical damage. For TGA-based FVF measurements, approximately 20 mg single-piece cylindrical specimens were sectioned due to the limited laminate thickness and to promote efficient heat transfer. Each specimen was carefully selected to ensure that it contained multiple tow interlacements of the twill architecture for ensuring mesostructural representativeness, which is a crucial aspect in such measurements. Thermal decomposition was analyzed using a TA Instruments Q-500 TGA. Neat epoxy, carbon fiber, and composite specimens were heated at 20°C min^{-1} under nitrogen at a constant flow rate of 100 mL min^{-1}. To eliminate residual oxygen that could promote carbon-fiber oxidation and lead to underestimation of fiber content, the furnace chamber was purged with nitrogen for 10 min at ambient temperature prior to testing. A reference temperature was selected at which matrix decomposition had stabilized and the residual mass remained essentially constant. By linking the mass-loss behavior of the composite with neat carbon-fiber specimens, the resin (matrix) weight fraction and the fiber weight fraction were determined using Equation (1). In this context, $W_{resin(\%)}$ denotes the proportion of resin in the composite, while Mass $loss_{composite(\%)}$ and Mass $loss_{carbonfiber(\%)}$ correspond to the measured mass losses of the composite and carbon fiber, respectively, up to the temperature at which the mass-loss rate becomes negligible and the residual mass stabilizes. The FVF for each specimen was subsequently calculated from the TGA-derived weight fractions using the known densities of the constituents, namely 1.17 g/cm^3 for the epoxy matrix and 1.77 g/cm^3 for the carbon fibers. Finally, the void content was evaluated for all specimens subjected to TGA-based resin burn-out testing. In this equation, ρ composite represents the experimentally measured composite density obtained from Archimedes' method, whereas W_{matrix} and W_{fiber} denote the matrix and fiber weight fractions, respectively [25, 26].

$$W_{resin}(\%) = \frac{\text{Mass loss}_{composite}(\%) - \text{Mass loss}_{carbonfiber}(\%)}{\text{Mass loss}_{epoxymatrix}(\%) - \text{Mass loss}_{carbonfiber}(\%)} \times 100 \quad (1)$$

$$V_f(\%) = \left(\frac{W_{fiber} / \rho_{fiber}}{W_{fiber} / \rho_{fiber} + W_{matrix} / \rho_{matrix}} \right) \times 100 \quad (2)$$

$$V_v(\%) = \left[1 - \rho_{composite} \left(\frac{W_{matrix}}{\rho_{matrix}} + \frac{W_{fiber}}{\rho_{fiber}} \right) \right] \times 100 \quad (3)$$

Figure 7 shows representative mass-loss rate curves as a function of temperature for the epoxy resin, carbon fiber, and the composite specimen, presented separately. More detailed information on the thermal degradation behavior of the individual constituents and composite samples can be found elsewhere [26]. Moreover, to complement density- and TGA-based void-content estimates and to visualize porosity morphology, representative coupons of approximately 10 × 10 mm^2 were cut

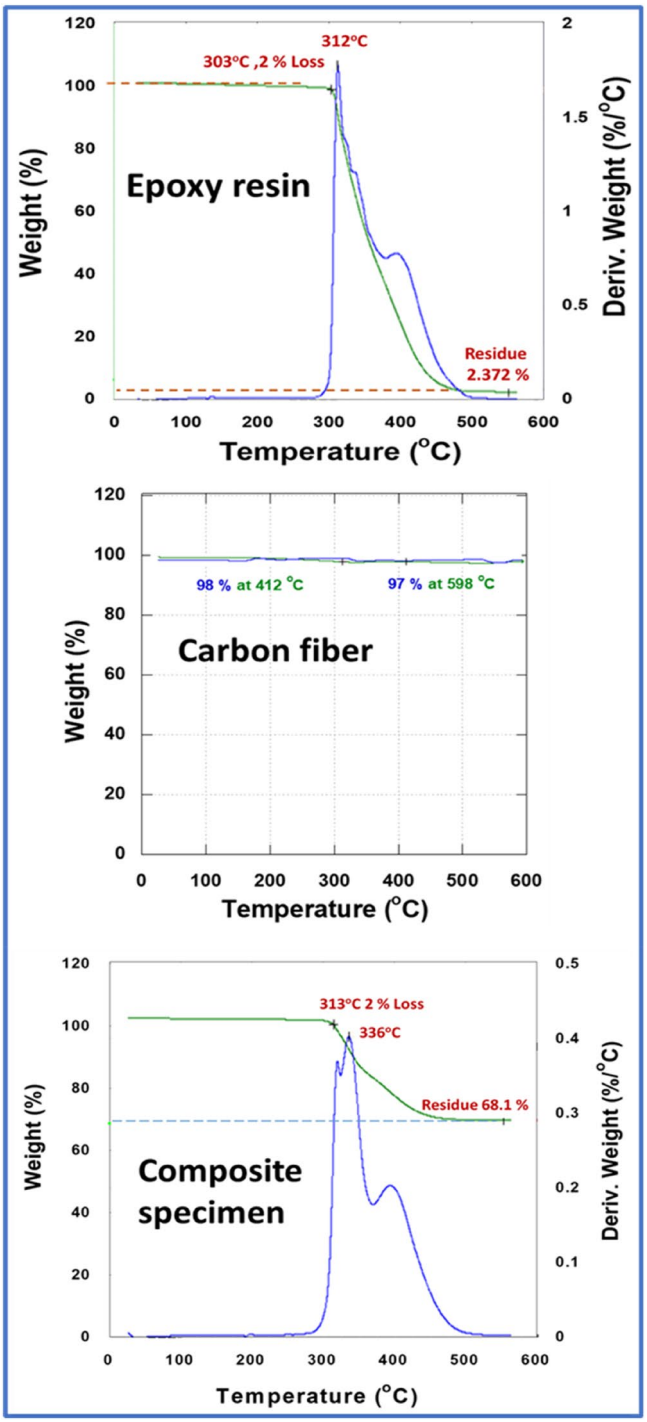

FIGURE 7 | Typical thermal degradation behavior of the composite specimen and its constituents, experimentally determined by TGA measurements.

from the central regions of selected laminates and examined using a micro-focus X-ray computed tomography (micro-CT) system (SkyScan 1172 Desktop, Bruker micro-CT, Kontich, Belgium). Scanning parameters were adapted from the literature to maximize contrast between carbon fibers [6–8]., the epoxy matrix, and voids, using no filter, a tube voltage of 62 kV, a current of 161 μA, a pixel size of 1.75–3 μm, and an image size of 4000 × 2096 pixels. Each specimen was scanned over a full 360° rotation, with a typical scan duration of approximately 2 h. Projection images were reconstructed in NRecon

with specimen-specific corrections, including misalignment compensation, ring-artifact reduction, and beam-hardening correction. Porosity was then segmented and quantified as the three-dimensional void volume fraction using CTAn (SkyScan). It should be noted that micro-CT was used primarily to corroborate inlet–outlet trends and to differentiate macro-voids from inter-tow porosity, rather than as the sole basis for reporting void content. The images are discussed in Section 3.

2.4 | Flexural Mechanical Properties

A three-point bending test was performed using an Instron Universal Testing Machine (Model 8810) equipped with a calibrated 10 kN load cell to evaluate the influence of processing methods on the flexural strength and modulus of the composite laminates. Tests were conducted on waterjet-cut specimens in accordance with ASTM D790-10, using a span-to-depth ratio of (32:1) and specimen dimensions of 25 mm in width and 80 mm in length. Care was taken during specimen preparation and positioning to ensure that the support and loading points did not coincide with critical local features of the woven architecture, such as tow crossover regions, to avoid biasing the measured response. Furthermore, the sectioned coupons were selected to contain multiple repeat units of the woven structure, thereby ensuring that the measured behavior reflects laminate-scale response rather than local variations associated with tow crimp and fiber waviness. Nevertheless, it is acknowledged that textile composites inherently exhibit mesostructural heterogeneity, which may contribute to some degree of scatter in the measured mechanical properties. Force vs. deflection at the center of the beam was recorded. The flexural strength, S, and the modulus values E_b were calculated using the equations as follows: [26].

$$S = \frac{3PL}{2bd^2}\left[1 + 6\left(\frac{D}{L}\right)^2 - 4\left(\frac{d}{L}\right)\left(\frac{D}{L}\right)\right] \tag{4}$$

where P is the applied load at the deflection point, L is the span length, d and b are the thickness and width of the specimen, respectively, and D is the deflection. The flexural modulus values, E_b, were calculated from Equation (4),

$$E_b = \frac{L^3 m}{4bd^3} \tag{5}$$

where m is the slope of the tangent to the initial straight-line portion of the load-deflection curve. Please be advised that, regardless of the process variants, the failure behavior of the laminates was systematically examined, and representative failure modes are presented in Figure 10a at the top. In all cases, failure predominantly initiated on the tensile side of the specimens, characterized by fiber fracture and matrix cracking at the bottom surface in the region of maximum bending moment, consistent with the classical bending response of fiber-reinforced composites. No evidence of compressive buckling or shear-dominated failure was observed for any sample within the selected test configuration. Note that flexural strength from three-point bending is inherently sensitive to thickness and surface conditions. The observed thickness differences are process-induced and therefore the results reflect the combined effect of material quality and consolidation rather than intrinsic properties alone.

3 | Results and Discussion

This study provides a critical comparison of six vacuum-assisted resin infusion variants, including C-VARTM, MAVIP, CAPRI, VAVI, PD-VARTM, and RTI with particular emphasis on thickness, density, FVF, void distribution, and mechanical performance along the laminate. To establish a consistent basis for comparison, consolidation behavior and flexural properties were evaluated at two matched locations for each laminate, specifically near the resin inlet and near the vacuum outlet. The results were first analyzed on a process-by-process basis to quantify inlet–outlet non-uniformity and subsequently to correlate thickness, density, FVF, and void content with the experimentally determined flexural strength and modulus. The discussion then extends to a cross-process comparison, using RTI as a high-quality benchmark to elucidate how specific process-control features govern consolidation quality and final structural performance.

Among the investigated techniques, C-VARTM exhibited the most pronounced process-induced inconsistencies. As shown in Figure 8a, a clear thickness gradient was observed, with the laminate having a thickness of 1.42 mm near the resin inlet and of 1.34 mm near the vacuum outlet. This inlet–outlet asymmetry directly reflects the non-uniform compaction pressure field inherent to passive vacuum infusion. As the resin front advances, local bag compaction and preform permeability evolve spatially, resulting in regions that consolidate differently across the panel. Figure 8b indicates slightly higher density on the vacuum side compared with the resin side. This behavior reflects the competing effects of increased consolidation toward the outlet and locally elevated void content, leading to density variations that remain smaller than the corresponding thickness differences. The combined thickness–density imbalance manifests more clearly in the FVF. Figure 9a reveals a substantial resin inlet–vacuum outlet FVF disparity of $\Delta = 6.70\%$, confirming that the thinner region near the vacuum outlet corresponds to a more highly compacted, fiber-rich laminate. Despite this higher consolidation level, C-VARTM also exhibits markedly uneven void content. As shown in Figure 9b, void content increases from 2.35% near the resin inlet to 4.55% near the vacuum outlet. These localized deficiencies promote entrapped voids and resin-rich zones that act as stress concentrators and compromise mechanical reliability. Consequently, although the vacuum-side region achieves a relatively high flexural strength of 700 MPa, the resin-side strength is limited to 620 MPa (Figure 10a,b). The agreement between these observations and prior studies underscores the need for improved flow-control and pressure-equalization strategies if C-VARTM is to approach aerospace-grade laminate quality.

MAVIP exhibited markedly improved laminate uniformity and structural integrity. Figure 9a shows an exceptionally low inlet–outlet FVF disparity of $\Delta = 0.44\%$, while Figure 8a indicates nearly identical thickness values of 1.39 mm and 1.37 mm at the resin and vacuum sides, respectively. These results point to uniform fiber wetting and minimal formation of resin-rich or dry regions. Correspondingly consistent density behavior is observed in Figures 8b and 9b confirms effective suppression of void formation across the laminate. Collectively, these trends demonstrate that MAVIP alleviates the resin inlet–vacuum

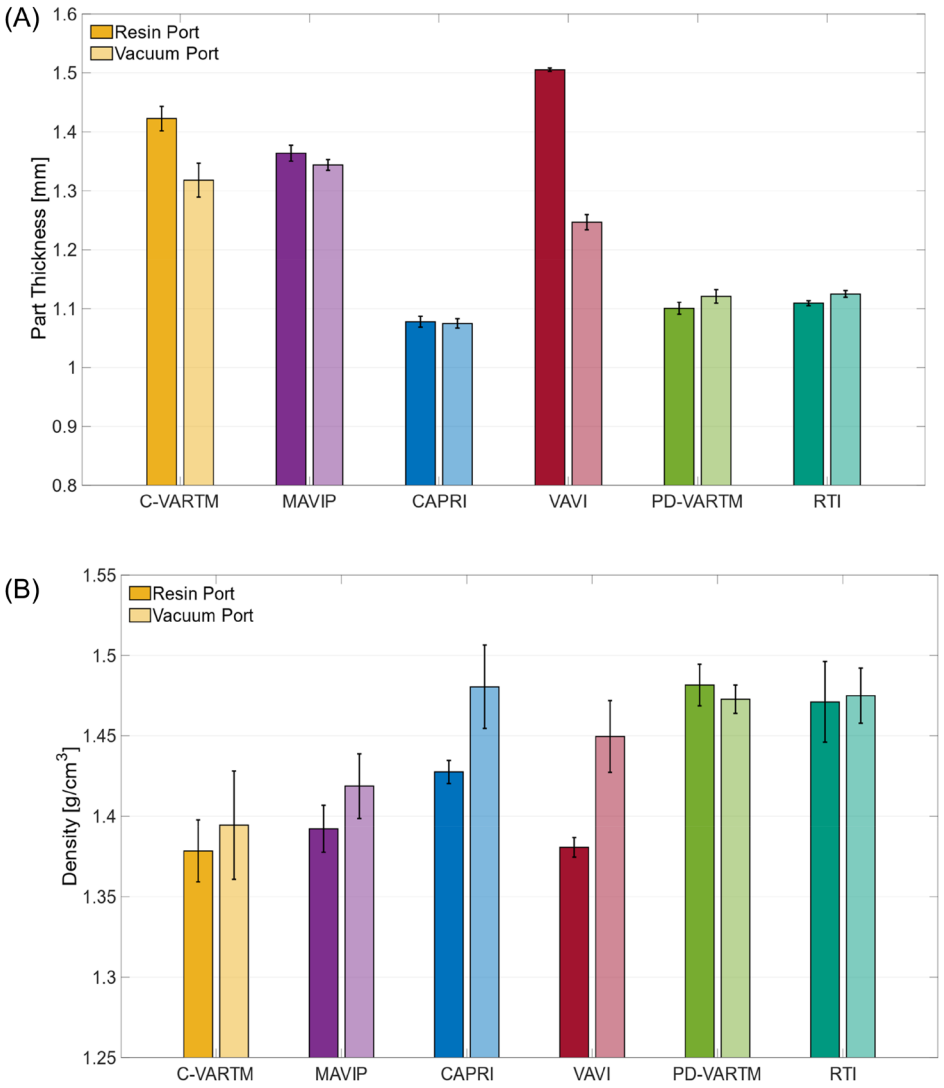

FIGURE 8 | (a) Part thickness of composite laminates manufactured by different processes, measured at regions near the resin port and vacuum port (b) Density of composite laminates manufactured by different processes, measured at regions near the resin port and vacuum port.

outlet consolidation imbalance characteristic of passive infusion. The semi-permeable membrane plays a central role in stabilizing the pressure field throughout the infusion cycle and enables continuous evacuation of air and volatiles even after resin breakthrough, thereby limiting late-stage void formation and race-tracking. The mechanical response mirrors this morphological uniformity, with flexural strengths of 671 and 631 MPa at the resin and vacuum sides, respectively (Figure 10a), and consistent stiffness trends in Figure 10b. Overall, MAVIP with a void content slightly higher than 2% emerges as a technically balanced and scalable infusion strategy that substantially narrows the gap between conventional vacuum infusion and autoclave-based processing.

CAPRI produced the most uniform laminates among the out-of-autoclave routes, with the lowest recorded thickness of approximately 1.09 mm (Figure 8a) and a correspondingly stable density response (Figure 8b), indicating a highly consolidated laminate with minimal inlet–outlet variability. The slightly lower density at the resin-port side of CAPRI may be attributed to localized differences in resin distribution and compaction during the initial impregnation stage. Transient pressure equilibration and local fiber bed relaxation near the inlet may lead to a marginally lower FVF, resulting in a reduced local density, despite the overall high consolidation quality of CAPRI. This geometric stability coincides with a high and consistent FVF of approximately 51% (Figure 9a) and suppressed void content in the range of 0.95%–1.45% (Figure 9b), in strong agreement with the findings of Niggemann et al. and Bréard et al. Although the reduced resin pressure inherently extends filling time, this drawback is offset by significantly improved impregnation and degassing performance. Mechanically, CAPRI laminates exhibited balanced flexural strengths of 698 MPa and 682 MPa at the resin and vacuum sides (Figure 10a), together with flexural moduli exceeding 41 GPa (Figure 10b), confirming its suitability for lightweight, high-strength structures requiring dimensional stability and internal homogeneity.

VAVI exhibited the greatest inconsistency in laminate quality. While the method achieved the highest local flexural strength in the study, which is 803 MPa on the vacuum side (Figure 10a), this local enhancement was accompanied by severe global non-uniformity. VAVI showed the largest inlet–outlet FVF asymmetry ($\Delta = 10.32\%$, Figure 9a) and a pronounced thickness

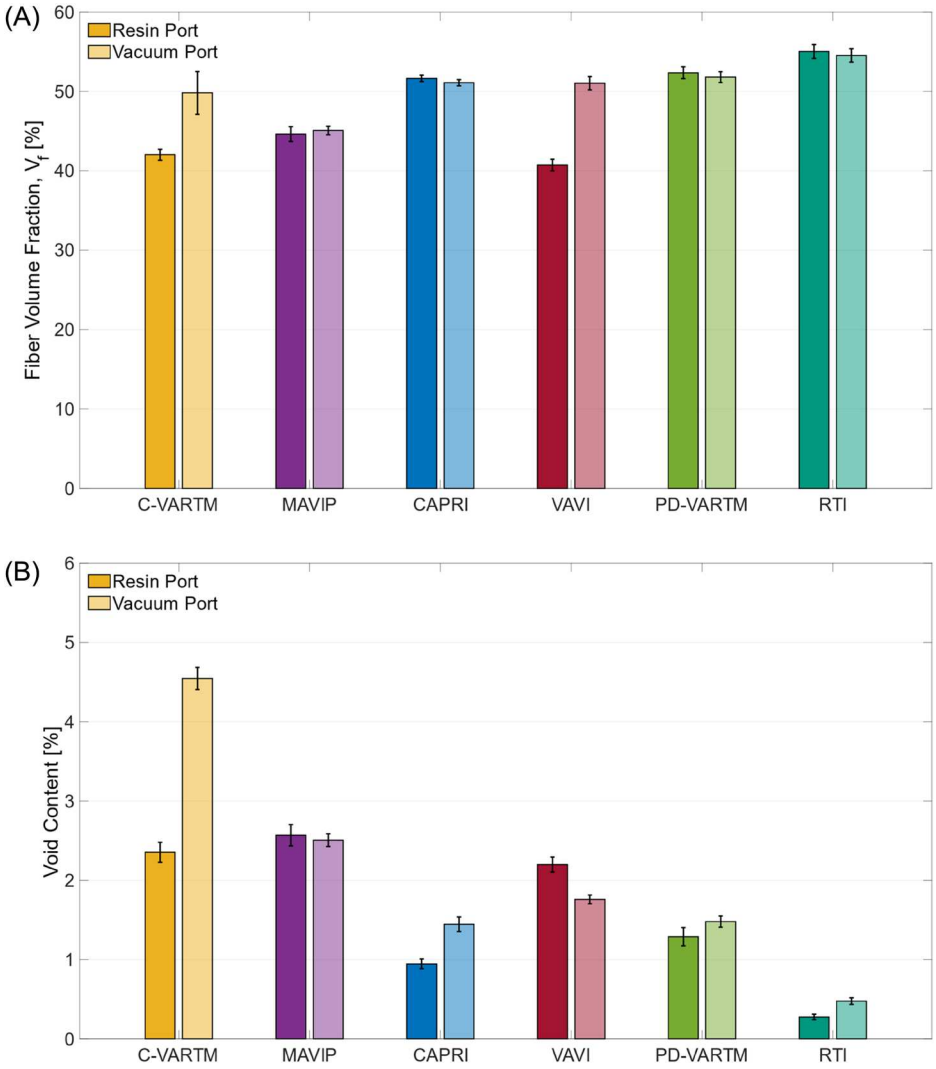

FIGURE 9 | (a) Fiber volume fraction of composite laminates manufactured by different processes, measured at regions near the resin port and vacuum port. (b) Void content of composite laminates manufactured by different processes, measured at regions near the resin port and vacuum port.

variation from 1.51 mm at the resin side to 1.27 mm at the vacuum side (Figure 8a). These findings are consistent with previous reports indicating that poorly tuned vibration parameters can destabilize the resin front and exacerbate process variability [26]. In the present study, these effects manifested as reduced resin-side flexural strength (562 MPa, Figure 10a) and a lower modulus of 38.9 GPa (Figure 10b). The accompanying density and void-content trends further support the conclusion that vibration-induced pressure fluctuations can amplify inlet–outlet variability rather than suppress it. Without real-time feedback and closed-loop control, vibration acts as a double-edged tool, enhancing local consolidation while undermining global laminate integrity.

PD-VARTM demonstrated a refined balance between performance and process simplicity. Thickness variation was minimal, with values tightly clustered between 1.11 and 1.13 mm (Figure 8a), and void contents confined to the 1.28%–1.48% range (Figure 9b). Density and FVF distributions were similarly uniform. Flexural strengths ranged from 714 to 747 MPa (Figure 10a), approaching CAPRI-level performance, while modulus trends confirmed a highly uniform consolidation state (Figure 10b). The key advantage of PD-VARTM lies in achieving near-CAPRI quality without the need for membranes or autoclave infrastructure, making it a scalable, low-barrier upgrade for conventional VARTM operations.

On the other hand, it should be distinctly emphasized that the flexural modulus exhibits a clear dependence on FVF across all processing routes. Laminates with lower FVFs, such as C-VARTM (around 42%) and MAVIP (around 45%), show comparatively lower modulus values varying from 36 to 40 GPa., while processes yielding higher FVFs, including CAPRI (around 51%), PD-VARTM (around 52%), and RTI (approximately 55%), demonstrate a consistent increase in stiffness, with modulus values reaching approximately 42 GPa, 48 GPa, and up to 55 GPa, respectively. This trend is consistent with classical composite laminate theory, where the elastic modulus is primarily governed by FVF. According to the rule of mixtures, the modulus increases with increasing fiber content. A similar relationship is also observed at the local scale, as evidenced by the inlet–outlet variations. For instance, in the VAVI process, the resin-port region with a lower FVF (around 40.5%) corresponds to a lower modulus of approximately 35 GPa, whereas the vacuum-port

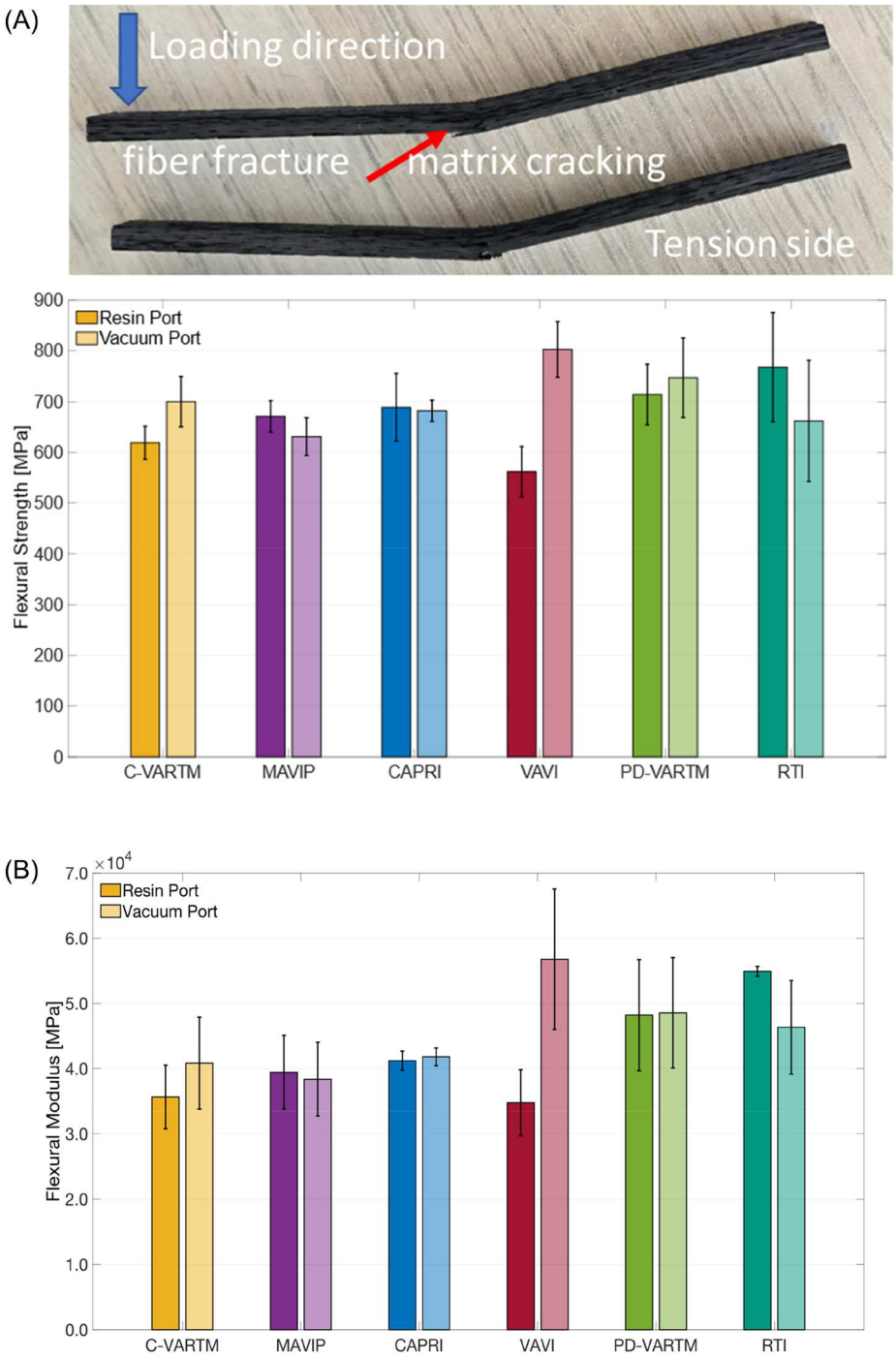

FIGURE 10 | (a) Flexural strength of composite laminates manufactured by different processes, measured at regions near the resin port and vacuum port. (b) Flexural modulus of composite laminates manufactured by different processes, measured at regions near the resin port and vacuum port.

region, with a higher FVF (around 51%), exhibits a significantly higher modulus of approximately 57 GPa. This further confirms that FVF is the dominant parameter controlling flexural stiffness, both globally across different processing routes and locally within the laminate.

Overall, among all routes, RTI consistently delivered the highest laminate quality. The integration of vacuum-assisted impregnation with pressure-assisted consolidation resulted in near-perfect thickness uniformity (around 1.12 mm, Figure 8a), stable density response (Figure 8b), FVF exceeding 55% (Figure 9a), and ultra-low void contents of 0.28%–0.48% (Figure 9b). These consolidation advantages translated directly into superior mechanical performance, with flexural strengths up to 768 MPa and moduli above 54 GPa (Figure 10a,b). Although RTI requires specialized infrastructure and careful control of stiff–soft region design, its performance aligns closely with fully autoclaved aerospace composites while offering greater flexibility in laminate thickness and processing window.

Figure 11 presents Micro-CT cross-sections that corroborate the bulk trends by revealing clear differences in porosity

morphology across the six infusion routes. Voids appear as low-attenuation dark regions. Discontinuities intersecting free surfaces were classified by CTAn as open pores; however, these features primarily stem from edge chipping and micro-cracking introduced during specimen sectioning. Accordingly, the CT images provide a microstructural rationale for the trends observed in the TGA-based void analysis and the corresponding density response. A semi-quantitative 2D analysis based on grayscale threshold segmentation of representative regions further confirms that porosity decreases systematically from C-VARTM to RTI, following the trend C-VARTM around 1.5, MAVIP around 0.8, VAVI around 0.55%, CAPRI around 0.45%, PD-VARTM around 0.32%, and RTI around 0.21%, in strong agreement with the bulk void contents obtained from burn-off measurements. It should be noted, however, that a direct quantitative correlation between CT-derived volumetric porosity and void content estimated from the density/burn-off method was not established in the present study, as the quantitative accuracy of CT strongly depends on scan resolution, thresholding strategy, segmentation quality, and the detectability of sub-resolution voids. Hence, the CT analysis was primarily employed for qualitative and semi-quantitative evaluation of internal defect distribution, whereas the density/burn-off approach was adopted as a cost-effective, practical, and well-established bulk method

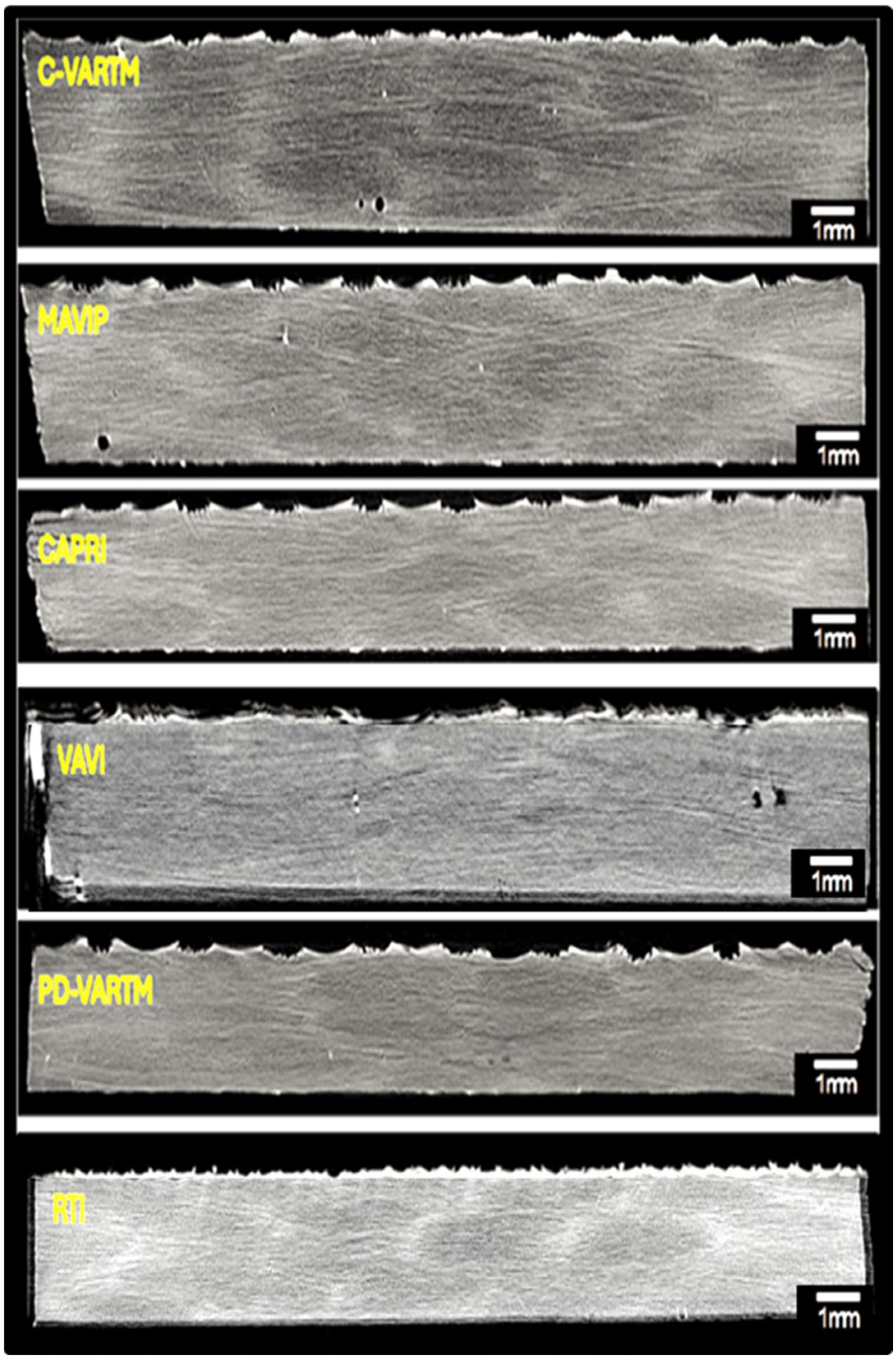

FIGURE 11 | Representative micro-CT cross-sectional slices of laminates produced via the six infusion routes. Images were reconstructed from a representative VOI of approximately $8 \times 8 \times 3\,mm^3$ at an isotropic voxel resolution of around $4\,\mu m$. Voids appear as low-attenuation dark regions.

for comparative void content assessment across the investigated laminates. Figure 9b C-VARTM shows distinct macro-voids within the laminate interior, typically as isolated rounded pores, consistent with higher void sensitivity under passive vacuum infusion. MAVIP and CAPRI exhibit cleaner cross-sections with fewer voids and a more uniform through-thickness morphology. VAVI displays a heterogeneous distribution, with voids concentrated in specific regions, consistent with localized consolidation gains alongside increased variability. This behavior suggests that vibration enhances local fiber bed compaction but does not ensure a globally uniform pressure field, leading to spatially heterogeneous void suppression. PD-VARTM and RTI show the most void-suppressed microstructures, with sparse, small, and isolated pores within the scanned volume of interest (VOIs), in line with superior consolidation quality. RTI remains the benchmark across both density and void-content datasets. Micro-CT mainly detects larger, resolvable voids within the selected VOIs, whereas the bulk void content in Figure 9b (from density and fiber-content measurements) also accounts for finer micro-porosity and resin-rich regions below the CT resolution. Consequently, while CT-derived values may underestimate the absolute porosity due to resolution limitations and sub-voxel defect detectability, they provide a robust representation of relative differences and demonstrate strong consistency with the bulk measurements. Together, Figures 9b and 11 establish a direct link between bulk quantification and void morphology, enabling a clear distinction between infusion routes exhibiting pronounced macro-voids and spatial non-uniformity and those achieving consistently low defect levels.

Figure 12 presents a multi-metric comparison of the six infusion routes at the resin inlet and vacuum outlet using radar plots. The plots were generated in MATLAB using min–max normalization, with each polygon representing a single process and integrating six performance metrics into a unified visual signature. Because the metrics differ in units and numerical range, all values were normalized globally using the combined dataset of resin inlet and vacuum outlet mean values across all processes. As a result, both radar plots share an identical scale, and differences in polygon size or shape between ports directly reflect true port-dependent behavior rather than independent rescaling. Since lower thickness and lower void content correspond to improved consolidation, the respective axes were inverted so that higher radial values consistently indicate more favorable outcomes across all metrics. The radar analysis clearly outlines three performance tiers. RTI exhibits the most expanded and well-balanced envelope across all metrics, indicating simultaneous optimization of consolidation quality and flexural performance. CAPRI closely follows, representing the strongest out-of-autoclave option with a consistently high envelope and minimal distortion between resin and vacuum ports. A defining characteristic of these routes is not isolated peak values, but the concurrent achievement of favorable consolidation indicators, strong mechanical performance, and reduced port sensitivity, supporting their role as reference-quality manufacturing routes when both structural performance and dimensional consistency are required. A second tier is formed by PD-VARTM and MAVIP, which display intermediate-to-high envelopes with more conservative extremes. Their principal advantage lies in the combination of competitive overall performance and comparatively stable behavior between resin and vacuum ports. Although their footprints do not reach the same extent as the top tier across all metrics, they avoid the pronounced expansion–contraction patterns observed in more variable processes, indicating a more predictable manufacturing outcome with lower infrastructure and process complexity. From a practical standpoint, these methods represent balanced candidates where manufacturability and scalability must be considered alongside performance. In contrast, C-VARTM and VAVI show the greatest deviation from uniformly expanded and symmetric profiles. Their radar plots reveal either generally reduced envelopes across multiple metrics or pronounced mismatches between resin inlet and vacuum-port responses, indicating that improvements achieved locally are not consistently reproduced throughout the laminate. This behavior reflects lower process robustness and highlights that process suitability cannot be inferred from a single favorable metric, as local gains may coincide with losses in consolidation-related attributes and increased port dependence. Overall, the radar-based evaluation supports a tiered interpretation in which RTI and CAPRI deliver the most uniform and spatially consistent multi-metric response, PD-VARTM and MAVIP provide robust, lower-complexity alternatives, and C-VARTM and VAVI exhibit the clearest signatures of process-induced variability, necessitating tighter control for use in high-reliability applications. VAVI exhibit the greatest variability and port dependence, highlighting the need for tighter control to meet high-reliability application requirements. Accordingly, the combined micro-CT validation and radar-based multi-metric benchmarking provide an integrated, defect-to-performance interpretation of process capability, linking porosity morphology and port sensitivity to the consolidation metrics and flexural responses discussed above. On this basis, RTI and CAPRI emerge as the most reliable routes when dimensional consistency and structural performance are jointly required, whereas PD-VARTM and MAVIP offer robust, lower-complexity alternatives, and C-VARTM and VAVI clearly require tighter control to meet high-reliability application demands.

It is worth noting that the behavior of the investigated processes may differ when applied to curved or geometrically complex structures rather than flat panels. In such configurations, factors such as non-uniform flow front progression, local permeability variations, and race-tracking along edges or thickness transitions may lead to increased heterogeneity in fiber–resin distribution. Previous studies have shown that these effects become more pronounced in non-planar geometries, potentially resulting in dry spots, void formation, and thickness-dependent resin accumulation. Within the framework of this study, in C-VARTM, increased flow path complexity and edge-driven race-tracking may lead to non-uniform impregnation and dry spots, particularly in regions with thickness variations or sharp curvatures. In CAPRI, the presence of a controlled pressure or counter-pressure field may improve flow stability; however, local permeability variations and tooling constraints can still affect uniform filling in complex geometries. MAVIP can offer improved pressure distribution and reduced void content; nevertheless, membrane compliance and local bridging effects may influence resin flow in highly curved regions. PD-VARTM may provide better control in flow rate and resin delivery, although its sensitivity to flow resistance changes in complex geometries can affect filling uniformity. VAVI may enhance resin infiltration and reduce void formation; however, its effectiveness depends on local geometry and fiber architecture,

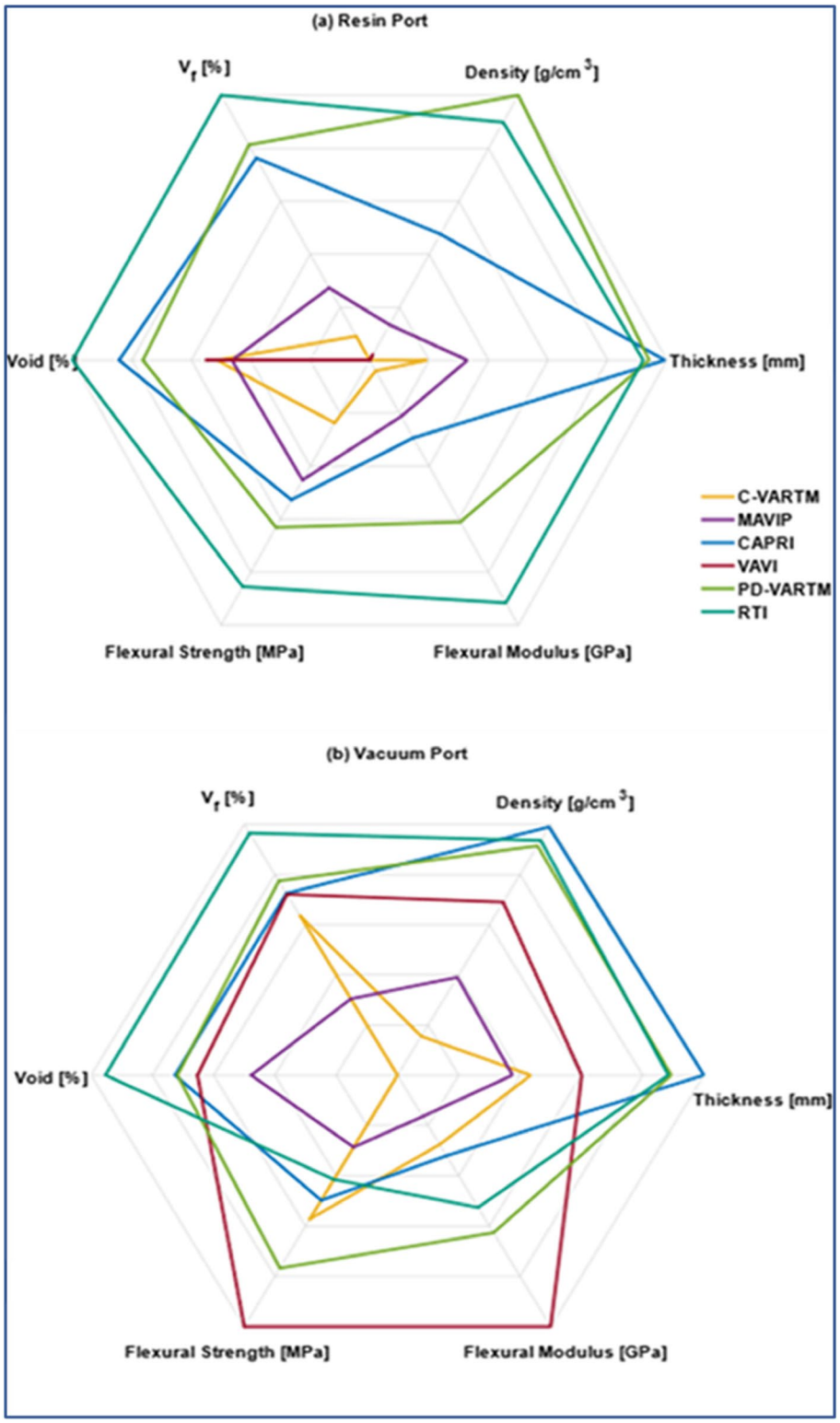

FIGURE 12 | Radar-plot comparison of consolidation quality and flexural performance for composite laminates manufactured by six infusion routes at (a) the resin port and (b) the vacuum port.

particularly in non-planar sections. In RTI processes performed under autoclave pressure, improved compaction and reduced void content can be achieved; however, the placement of injection and venting points (soft points) becomes more critical, as improper positioning in complex geometries may lead to non-uniform flow, delayed impregnation, or local dry regions. Among the investigated processes, RTI and MAVIP are expected to provide more reliable performance in curved geometries due to improved pressure control and compaction, whereas conventional VARTM-based approaches are more prone to flow-induced defects under such conditions. While the present study focuses on flat panels to enable a controlled comparison, these aspects should be considered when extending the processes to more complex structural components.

4 | Conclusions

This study delivered a quantitative and spatially resolved comparison of six vacuum-assisted resin infusion variants, including C-VARTM, MAVIP, CAPRI, VAVI, PD-VARTM, and RTI, by systematically assessing inlet–outlet variability in thickness, density, FVF, void content, and flexural performance. Flexural strength was considered as the primary performance indicator distinguishing the investigated process variants and reflects the combined influence of FVF, void content, and structural uniformity. Significant differences were observed between processes based on resin inlet and vacuum outlet regions. C-VARTM exhibited a nearly 13% variation in flexural strength across the panel, while VAVI achieved the highest local strength (803 MPa) but with pronounced spatial inconsistency. In contrast, MAVIP and PD-VARTM demonstrated more stable mechanical responses, with flexural strengths ranging between 631–671 MPa and 714–747 MPa, respectively. CAPRI and RTI consistently delivered high and spatially uniform strength values, with RTI reaching up to 768 MPa, highlighting the importance of process controllability over isolated peak performance.

These variations in mechanical performance are directly governed by FVF and its strong influence on flexural modulus. Laminates with lower FVF, such as C-VARTM (around 42%) and MAVIP (around 45%), exhibit comparatively lower stiffness, with modulus values between 36 GPa and 40 GPa. In contrast, higher-FVF processes, including CAPRI (around 51%), PD-VARTM (around 52%), and RTI (around 55%), show a systematic increase in stiffness, reaching approximately 42 GPa, 48 GPa, and up to 55 GPa, respectively. This behavior is consistent with classical composite laminate theory, where stiffness scales with fiber content according to the rule of mixtures. The same relationship is also evident locally in a manner that, in the VAVI process, a resin-port region with lower FVF (around 40.5%) corresponds to a modulus of approximately 35 GPa, whereas a vacuum-port region with higher FVF (around 51%) reaches values as high as 57 GPa. These findings confirm that FVF is the dominant parameter controlling flexural stiffness both globally and locally within the laminate.

The observed mechanical trends are further linked to process-induced thickness gradients and consolidation uniformity. C-VARTM and VAVI exhibited pronounced inlet–outlet asymmetry, with FVF differences of 6.7% and 10.3%, respectively, accompanied by thickness variations up to 6% and exceeding 15%. In contrast, MAVIP and PD-VARTM effectively minimized these gradients, maintaining FVF differences below 1% and near-uniform thickness distributions. CAPRI and RTI provided the highest level of dimensional stability, producing laminates with nearly constant thickness (1.09 and ~1.12 mm, respectively), reflecting superior process control and consolidation efficiency.

Void content was found to play a critical role in determining both the magnitude and consistency of flexural performance. C-VARTM exhibited the highest void sensitivity, with void content increasing from 2.35% at the resin inlet to 4.55% at the vacuum outlet. VAVI, despite achieving high local strength, showed increased heterogeneity in defect distribution. In contrast, MAVIP and PD-VARTM reduced void content to approximately 1.3% and 1.5%, while CAPRI and RTI achieved the lowest levels, with CAPRI below 1.5% and RTI reaching ultra-low values of 0.28%–0.48%. These reductions directly enhance load transfer efficiency and reduce mechanical scatter, contributing to improved laminate reliability.

Micro-CT observations further corroborate these findings by revealing clear differences in void morphology and spatial distribution. A semi-quantitative analysis based on grayscale threshold segmentation indicates a systematic decrease in porosity from C-VARTM (1.5%) to MAVIP (0.8%), VAVI (0.55%), CAPRI (0.45%), PD-VARTM (0.32%), and RTI (0.21%), in strong agreement with bulk void content trends obtained from density/burn-off measurements.

Overall, RTI and CAPRI demonstrate the most balanced and high-performance processing routes, combining high FVF, low void content, minimal thickness variation, and consistently high mechanical performance. Among them, RTI emerges as the most effective method, achieving FVFs exceeding 55%, flexural strengths up to 768 MPa, and modulus values above 54 GPa, together with near-perfect thickness uniformity and ultra-low void content. PD-VARTM and MAVIP provide robust intermediate solutions with improved process stability and reduced variability, while C-VARTM and VAVI exhibit significant sensitivity to process conditions and spatial non-uniformity. These findings confirm that minimizing inlet–outlet variability is a key requirement for achieving aerospace-grade laminate quality and provide a quantitative framework for selecting infusion strategies based on performance, robustness, and processing complexity.

By the way, it should be noted that the present study is based on relatively thin laminates, providing a controlled basis for comparing process-induced variability. While this enables consistent evaluation across different infusion routes, thicker aerospace-grade laminates may involve additional effects such as through-thickness flow limitations and evolving compaction behavior. Therefore, direct extrapolation to large-scale structures should be made with caution, and future work will address process scalability in thicker configurations.

Author Contributions

Ilhan Kahraman: investigation, writing – original draft, validation, methodology, software, formal analysis. **Nilperi Uysal:** conceptualization, investigation, methodology, data curation, software, validation. **Çağlar Subaşı:** investigation, validation, data curation, conceptualization, methodology, writing – review and editing. **Selin Dursun:** conceptualization, investigation, software, resources, data curation, methodology. **Muhammet İskender:** conceptualization, investigation, formal analysis. **Özgü Çalın:** validation, investigation, formal analysis. **Uğur Şimşir:** methodology, resources. **Hatice S. Sas:** conceptualization, investigation, writing – original draft, writing – review and editing, data curation, software, methodology, validation, supervision, resources, project administration, funding acquisition, visualization. **A. Tuğrul Seyhan:** conceptualization, investigation, writing – original draft, writing – review and editing, validation, methodology, data curation, supervision, resources, funding acquisition, project administration.

Acknowledgments

This work was supported by the Scientific and Technological Research Council of Türkiye (TÜBİTAK) under grant numbers 218M297 and 22AG001.

Funding

This work was supported by Türkiye Bilimsel ve Teknolojik Araştırma Kurumu.

Data Availability Statement

The data that support the findings of this study are available from the corresponding author upon reasonable request.

References

1. P. K. Mallick, *Composite Engineering Handbook* (CRC Press, 1997).

2. K. T. Hsiao, J. W. Gillespie, Jr., S. G. Advani, and B. K. Fink, "Role of Vacuum Pressure and Port Locations on Flow Front Control for Liquid Composite Molding Processes," *Polymer Composites* 22 (2001): 660–668, https://doi.org/10.1002/pc.10568.

3. A. T. Seyhan, "A Statistical Study of Fatigue Life Prediction of Fibre Reinforced Polymer Composites," *Polymers and Polymer Composites* 19 (2011): 717–724, https://doi.org/10.1177/096739111101900901.

4. A. Gilliot, "Matrix Influence on the Impact Tolerance of Carbon Composites Made of Non-Crimp Fabric. DLR-Forschungsbericht. DLR-FB 2010-03," Dissertation, Otto-von-Guericke University, Magdeburg. 140 S, 2010.

5. R. Mathur, D. Heider, C. Hoffmann, J. W. Gillespie, Jr., S. G. Advani, and B. K. Fink, "Flow Front Measurements and Model Validation in the Vacuum Assisted Resin Transfer Molding Process," *Polymer Composites* 22 (2001): 477–490.

6. M. H. Arikan, F. Eroglu, V. Eskizeybek, E. F. Sukur, M. Yildiz, and H. S. Sas, "A Systematic Characterization Approach for Vacuum Bag Only Prepregs Towards an Accurate Process Design," *Materials* 15 (2022): 451–461, https://doi.org/10.3390/ma15020451.

7. C. Centea and P. Hubert, "Measuring the Impregnation of an Out-Of-Autoclave Prepreg by Micro-CT," *Composites Science and Technology* 71 (2011): 593–599, https://doi.org/10.1016/j.compscitech.2010.12.009.

8. J. J. Torres, M. Simmons, F. Sket, and C. González, "An Analysis of Void Formation Mechanisms in Out-Of-Autoclave Prepregs by Means of X-Ray Computed Tomography," *Composites Part A: Applied Science and Manufacturing* 117 (2019): 230–242, https://doi.org/10.1016/j.compositesa.2018.11.020.

9. M. Bodaghi, R. Costa, R. Gomes, J. Silva, N. Correia, and F. Silva, "Experimental Comparative Study of the Variants of High-Temperature Vacuum-Assisted Resin Transfer Molding," *Composites Part A Applied Science and Manufacturing* 129 (2020): 105708–105721, https://doi.org/10.1016/j.compositesa.2019.105708.

10. M. Mehdikhani, L. Gorbatikh, I. Verpoest, and S. V. Lomov, "Voids in Fiber-Reinforced Polymer Composites: A Review on Their Formation, Characteristics, and Effects on Mechanical Performance," *Journal of Composite Materials* 53 (2019): 1579–1669, https://doi.org/10.1177/0021998318772152.

11. H. Yurdakul, O. Durukan, A. T. Seyhan, H. Celebi, R. M. Oksuzoglu, and S. Turan, "Microstructural Characterization of Corn Starch-Based Porous Thermoplastic Composites Filled With Multiwalled Carbon Nanotubes," *Journal of Applied Polymer Science* 127 (2013): 812–820, https://doi.org/10.1002/app.37794.

12. S. G. Advani and E. M. Sozer, *Process Modeling in Composite Manufacturing* (CRC Press, 2010).

13. T. Chang, L. Zhan, W. Tan, and S. Li, "Effect of Autoclave Pressure on Interfacial Properties at Micro- and Macro-Level in Polymer-Matrix Composite Laminates," *Fibers and Polymers* 18 (2017): 1614–1622, https://doi.org/10.1007/s12221-017-7384-4.

14. D. Abraham, S. Matthews, and R. McIlhagger, "A Comparison of Physical Properties of Glass Fibre Epoxy Composites Produced by Wet Lay-Up With Autoclave Consolidation and Resin Transfer Moulding," *Composites Part A: Applied Science and Manufacturing* 29, no. 7 (1998): 795–801, https://doi.org/10.1016/S1359-835X(98)00055-4.

15. P. K. Mallick, *Processing of Polymer Matrix Composites* (CRC Press, 2018).

16. M. Li, Y. Li, Z. Zhang, and Y. Gu, "Pressure Window Analysis for Thin Laminated Composites in Autoclave Process," *Polymer Composites* 30 (2009): 169–175, https://doi.org/10.1002/pc.20547.

17. A. Hindersmann, "Confusion About Infusion: An Overview of Infusion Processes," *Composites Part A: Applied Science and Manufacturing* 126 (2019): 105583, https://doi.org/10.1016/j.compositesa.2019.105583.

18. S. van Oosterom, T. Allen, M. Battley, and S. Bickerton, "An Objective Comparison of Common Vacuum Assisted Resin Infusion Processes," *Composites Part A: Applied Science and Manufacturing* 125 (2019): 105528, https://doi.org/10.1016/j.compositesa.2019.105528.

19. X. Sun, S. Li, and L. J. Lee, "Mold Filling Analysis in Vacuum-Assisted Resin Transfer Molding. Part I: SCRIMP Based on a High-Permeable Medium," *Polymer Composites* 19 (1998): 807–814, https://doi.org/10.1002/pc.10155.

20. W. Li, J. Krehl, J. W. Gillespie, Jr., et al., "Process and Performance Evaluation of the Vacuum-Assisted Process," *Journal of Composite Materials* 38 (2004): 1803–1814, https://doi.org/10.1177/0021998304044769.

21. C. Niggemann, Y. S. Song, J. W. Gillespie, Jr., and D. Heider, "Experimental Investigation of the Controlled Atmospheric Pressure Resin Infusion (CAPRI) Process," *Journal of Composite Materials* 42 (2008): 1049–1061, https://doi.org/10.1177/0021998308090650.

22. M. A. Yalcinkaya, E. M. Sozer, and M. C. Altan, "Effect of External Pressure and Resin Flushing on Reduction of Process-Induced Voids and Enhancement of Laminate Quality in Heated-VARTM," *Composites Part A: Applied Science and Manufacturing* 121 (2019): 353–364, https://doi.org/10.1016/j.compositesa.2019.03.040.

23. M. A. Yalcinkaya, E. M. Sozer, and M. C. Altan, "Fabrication of High Quality Composite Laminates by Pressurized and Heated-VARTM," *Composites Part A: Applied Science and Manufacturing* 102 (2017): 336–346, https://doi.org/10.1016/j.compositesa.2017.08.017.

24. H. S. Sas and M. Erdal, "Modeling of Particle–Resin Suspension Impregnation in Compression Resin Transfer Molding of Particle-Filled, Continuous Fiber Reinforced Composites," *Heat and Mass Transfer* 50 (2014): 397–414, https://doi.org/10.1007/s00231-013-1275-z.

25. A. Aruniit, H. Herranen, and K. Miller, "Comparative Study of the VARTM, VAP and MTI Vacuum Infusion Processes," *Key Engineering Materials* 674 (2016): 71–76, https://doi.org/10.4028/www.scientific.net/KEM.674.71.

26. N. Meier, I. Kahraman, A. T. Seyhan, S. Zaremba, and K. Drechsler, "Evaluating Vibration Assisted Vacuum Infusion Processing of Hexagonal Boron Nitride Sheet Modified Carbon Fabric/Epoxy Composites," *Composites Science and Technology* 128 (2016): 94–103, https://doi.org/10.1016/j.compscitech.2016.03.022.

27. A. Tuna, I. Kahraman, M. Akdere, et al., "A Proof-Of-Concept Study on Sustainably Upcycled Chicken Feather Fibers as Interfacial Modifiers and Complementary Fillers in Multiscale Carbon/Epoxy Composites," *Polymer Composites* 47, no. 8 (2025): 7136–7154, https://doi.org/10.1002/pc.70612.

28. A. D. Kelkar and J. S. Tate, "Low-Cost Manufacturing of Textile Composites Using Vacuum-Assisted Resin Transfer Molding," *Proceedings of the 20th All India Manufacturing Technology, Design and Research Conference* 1 (2002): 712–716.

29. Bombardier Aerospace, "Final report – Resin Infusion Technology," Technical Report, (2010) https://s44864.pcdn.co/wp-content/uploads/archive-issues/september-2010.pdf.

30. G. Gardiner, "Bombardier wins award for resin transfer infusion wing" Composite World. (2019) https://www.compositesworld.com/news/bombardier-wins-uk-royal-academy-of-engineering-award-for-resin-transfer-infusion-wing.

31. X. Fu, C. Zhang, R. Liang, B. Wang, and J. C. Fielding, "High Temperature Vacuum-Assisted Resin Transfer Molding of Phenylethynyl Terminated Imide Composites," *Polymer Composites* 32 (2011): 52–58, https://doi.org/10.1002/pc.21015.

32. L. Liu, B. M. Zhang, D. F. Wang, and Z. J. Wu, "Effects of Cure Cycles on Void Content and Mechanical Properties of Composite Laminates," *Composite Structures* 73 (2006): 303–309, https://doi.org/10.1016/j.compstruct.2005.02.001.